Tectonics

RESEARCH ARTICLE
10.1029/2020TC006663

Key Points:

- D. João de Castro seamount in the Terceira Rift, Azores is influenced by a SW-NE regional transtensional and a local radiating stress field
- Structural, seismic, and geochemical data imply formation by the growth of volcanic ridges along with local stress field changes
- The geometry, chemistry, and rifting rates of the Terceira Rift are more comparable to continental rifts rather than mid-ocean ridges

Supporting Information:

Supporting Information may be found in the online version of this article.

Correspondence to:

R. Romer,
rene.romer@fau.de

Citation:

Romer, R. H. W., Beier, C., Haase, K. M., Eberts, A., & Hübscher, C. (2021). The evolution of central volcanoes in ultraslow rift systems: Constraints from D. João de Castro seamount, Azores. *Tectonics*, *40*, e2020TC006663. https://doi.org/10.1029/2020TC006663

Received 16 DEC 2020
Accepted 8 MAR 2021

The Evolution of Central Volcanoes in Ultraslow Rift Systems: Constraints From D. João de Castro Seamount, Azores

R. H. W. Romer[1], C. Beier[2], K. M. Haase[1], A. Eberts[1,3], and C. Hübscher[4]

[1]GeoZentrum Nordbayern, Friedrich-Alexander-Universität Erlangen-Nürnberg, Erlangen, Germany, [2]Department of Geosciences and Geography, Research Programme of Geosciences and Geography (GeoHel), University of Helsinki, Helsinki, Finland, [3]Landesamt für Geologie und Bergbau Rheinland-Pfalz, Mainz, Germany, [4]Institut für Geophysik, Universität Hamburg, Hamburg, Germany

Abstract The Dom João de Castro seamount in the Hirondelle Basin (Azores) is a central volcano on the ultraslow diverging Terceira Rift axis. The combination of structural and geochemical data provides insights into the evolution of central volcanoes in oceanic rift systems above the Azores melting anomaly. The orientation of fault scarps and volcanic structures at D. João de Castro and the adjacent Castro fissure zone indicate that the regional SW-NE extending stress field dominates the morphology of the NW Hirondelle Basin. The regional tectonic stress field controls the crustal melt pathways and leads to dike emplacement along fissure zones and the prevalent eruption of mafic lavas. The occurrence of mafic to felsic lavas at D. João de Castro gives evidence for both a deep and a shallow crustal melt reservoir generating a subordinate local stress field at the seamount. New Sr-Nd-Pb isotope data along with incompatible trace element ratios indicate that D. João de Castro and the Castro Ridges originated from similarly heterogeneous mantle source but did not form simultaneously. Our new model implies that central volcanoes along the Terceira Rift form by the growth of volcanic ridges and transitioned into circular edifices after magmatic systems generate local changes in the regional lithospheric stress field. The geometry of D. João de Castro and other magmatic systems along the Terceira Rift combined with the alkaline nature of the erupted lavas, and the large lithosphere thickness indicates that young oceanic rifts are more similar to continental rifts rather than mid-ocean ridges.

Plain Language Summary Dom João de Castro seamount is a large submarine volcano located in the submarine Hirondelle Basin in the Azores archipelago. The Hirondelle Basin is formed as a result of extensional forces in the oceanic crust along the Azorean Terceira Rift that causes rifting of the Eurasian and Nubian plates. The presence of the D. João de Castro volcano and several elongated volcanic ridges inside the basin shows that the extensive magmatic activity in the Azores contributes to the opening of the basin. By quantifying the orientations of the tectonic and volcanic structures in the basin, it can be shown that the formation is controlled by a dominant SW-NE directed extensional stress combined with extensive magmatic activity. Based on combined structural and geochemical observations, we conclude that the D. João de Castro seamount formed from the growth of elongated volcanic ridges and transitioned into a circular edifice after a magma system generates a local change in the crustal stress field. The geometry and geochemical composition of volcanic rocks from the D. João de Castro magmatic system, as well as other magmatic systems along the Terceira Rift are more similar to continental rift systems rather than oceanic spreading centers.

1. Introduction

Volcanic activity along diverging plate boundaries in oceanic and continental settings commonly is the result of interacting magmatic and tectonic processes. Magmatism at oceanic and continental rift systems and mid-ocean ridges (MOR) plays a significant role in global plate tectonics, for example, leading to continental breakup and new oceanic crust formation (Heezen, 1960; Wilson, 1968). MORs as well as oceanic and continental rifts erupt a variety of chemically distinct lavas and have different morphological appearances depending among other processes on the extension rate. Fast-spreading MORs, for example, the East Pacific Rise (EPR), have continuous volcanically active segments and erupt large volumes of melt from the depleted

upper mantle forming symmetrical axial heights (Carbotte & Macdonald, 1994; Perfit & Chadwick, 1998). In contrast, slow-diverging continental rift systems and slow-spreading oceanic ridges, for example, the Southwest Indian Ridge (SWIR; Dick et al., 2003), erupt primitive lavas with a large overall chemical variability (Rubin & Sinton, 2007) but volcanic activity occurs rarely and scattered (Mendel et al., 2003). The temporal quiescence of volcanism in slowly diverging systems results in magmato-tectonic cycles of volcanic construction and tectonic phases forming axial valleys and basins in both oceanic (Mendel et al., 2003) and continental rift settings (Ebinger et al., 2013). Slow-rifting oceanic and continental systems are often characterized by alternating amagmatic and magmatic sections, for example, deep rift valleys are separated by volcanically active regions (Acocella, 2014; Michael et al., 2003). Here, most volcanic activity occurs in the center of a magmatic segment (Cannat et al., 1995) and lack of volcanism at the segment's edges implies transport of small degree melts from the sides toward the center (Carbotte et al., 2015). Magmato-tectonic segments in continental rifts, for example, in the Main Ethiopian Rift (MER) can be distinguished based on the type of deformation occurring during rift evolution, where the extension in the center of each segment is induced by magmatic intrusion. In contrast, at the extremities of the segments, the influence of diking decreases and deformation mainly occurs by tectonic faulting (Kurz et al., 2007).

The geochemical signatures of the lavas erupting in slowly diverging environments yield essential insights into crustal ascent conditions (Schwarz et al., 2004), mantle melting processes (Shen & Forsyth, 1995), and also reflect the chemical heterogeneity of the mantle (Shirey et al., 1987). The tectonic forces in these rift systems are manifested in tectonic structures, for example, several tens of kilometers long rift basins forming segments along MORs (Dick et al., 2003; Mutter & Karson, 1992) and continental rift systems (Hayward & Ebinger, 1996). Tectonic stresses are also a major controlling factor on the pathways of melts in the crust and influence the morphology of volcanic structures on the scale of a single edifice (Acocella & Neri, 2009). In slowly diverging continental and oceanic rift systems, focused magmatism leads to the formation of central volcanoes (Acocella, 2014). These are the surface expression of processes with an origin in the mantle and the crust, and thus, yield important insights into the evolution of rift systems. In this study, we focus on the evolution of central volcanoes in slow-diverging rift systems and on the related mantle-derived and crustal processes.

The Terceira Rift in the Eastern Azores Plateau combines features of both slow-spreading oceanic ridges and continental intraplate rift systems (Beier et al., 2008). It allows studying the evolution of a rift system with active volcanism from melting beneath variably thick lithosphere. The volcanic centers along the Terceira Rift are formed from melting of a geochemically anomalous mantle potentially associated with a small, thermal mantle plume (Beier et al., 2012; Bonatti, 1990; Gente et al., 2003; Madureira et al., 2005; Métrich et al., 2014; Montelli et al., 2004; Moreira et al., 2018; O'Neill & Sigloch, 2018; Schilling, 1975; White et al., 1976; Yang et al., 2006), which allows investigating mantle source heterogeneity and variation of melting conditions with respect to changing lithosphere thicknesses. The D. João de Castro seamount is a young, central volcano located right at the center of the active Terceira Rift and represents the only solitary central volcano along the entire rift formed from melting of the anomalous Azores mantle (Béguelin et al., 2017; Beier et al., 2008). The term central volcano here refers to a polygenetic volcano, which in the case of the Azores are stratovolcanoes with or without calderas (e.g., Sete Cidades on São Miguel, Santa Bárbara on Terceira Island). D. João de Castro volcano is therefore ideally suited to investigate the formation and evolution of central volcanoes in an active, slowly diverging oceanic rift system due to its transitional nature between rift systems and a central volcano.

Here, we use both geochemical and structural data to disentangle the influence of both mantle and crustal processes that are important during volcano formation and rift evolution. We show that the opening of the Terceira Rift results in the formation of several magmatic segments with volcanism concentrated at their centers leading to the formation of one or more central volcanic edifices. We propose a model based on volcano-tectonic features from the D. João de Castro seamount showing that central volcanoes along the Terceira Rift are formed from growth and merging of single volcanic ridges accompanied by changes in the tectonic stress field. The geometry of the D. João de Castro and other magmatic systems along the Terceira Rift in combination with the slow diverging rate, the alkaline nature of the erupted lavas, and the large crustal and lithosphere thickness indicates that the Terceira Rift is more similar to continental rift systems than to MORs.

2. Geological Setting

The Azores archipelago in the central North Atlantic is separated by the Mid-Atlantic Ridge (MAR) into an eastern (Figure 1a) and western part. The eastern Azores Plateau is bordered by the Terceira Rift in the north. Three volcanically active islands (Graciosa, Terceira and São Miguel) and two seamounts (D. João de Castro and East Formigas High, Figure 1a) are located on the Terceira Rift. The Azores Plateau as a whole formed above a melting anomaly in the mantle, either due to extensive melting of a small thermal plume head (Cannat et al., 1999; Schilling, 1975; White et al., 1976) or of an anomalous volatile-rich mantle (Asimow et al., 2004; Beier et al., 2012; Bonatti, 1990; Métrich et al., 2014; O'Neill & Sigloch, 2018; Schilling et al., 1980). The Terceira Rift is interpreted as an ultraslow oblique spreading axis, with a divergence rate of 2–4 mm/a (Luis & Miranda, 2008; Vogt & Jung, 2004), forming part of the diffuse plate boundary between the Eurasian and Nubian plates (Marques et al., 2013; Miranda et al., 2018; Sibrant et al., 2014). The relatively thick lithosphere and the lack of a systematic magnetic pattern parallel to the Terceira Rift, however, are contradictory to the occurrence of seafloor spreading in the rift (Storch et al., 2020). The young volcanic islands of the eastern Azores formed along the Terceira Rift or its predecessors (Krause & Watkins, 1970). The volcanic structures along the Terceira Rift occur in discrete tectonic segments with a regular spacing of 80–100 km (Lourenço et al., 1998) and are separated by deep nonvolcanic basins (Figure 1a, Beier et al., 2008). Volcanic fissure zones follow the trend of the tectonic structures and are observed at most islands and seamounts in the eastern Azores (Beier et al., 2017; Casalbore et al., 2015; Casas et al., 2018; Hildenbrand et al., 2014; Hübscher et al., 2016; Marques et al., 2015; Romer et al., 2018, 2019; Sibrant et al., 2014, 2016; Weiß, Hübscher, Wolf, et al., 2015). Eruptions from volcanic fissure zones either occur subaerially or submarine forming several kilometer-long volcanic ridges that are either isolated or at the submarine island flanks. Volcanism at the central volcanoes and fissure zones in the eastern Azores is primarily controlled by the regional tectonic stress fields, evident from the WNW-ESE and NW-SE elongated shaped islands and ridges (Hildenbrand et al., 2014; Lourenço et al., 1998). The D. João de Castro seamount is a central volcano located in the center of the Hirondelle Basin associated with volcanic ridges and cones above an active fissure zone (Figure 1b). The age of the oceanic lithosphere at D. João de Castro is between 24 Ma and 34 Ma (chrons 6C and 13 of the MAR; Cande & Kent, 1995) and the corresponding lithosphere thickness ranges from 50 to 60 km. Seismic tomography models of Spieker et al. (2018) display anomalously thick oceanic crust and overall much thicker lithosphere for the neighboring islands of Terceira and São Miguel both situated on lithosphere of up to 80-km thickness. This together with geochemical modeling at D. João de Castro indicating the presence of residual garnet in the mantle, that is, melting at >80 km (Beier et al., 2008; Robinson & Wood, 1998), shows that the lithosphere is thicker than normal oceanic lithosphere. The seamount's age is estimated to be <0.5 Ma, whereas lavas from the adjacent NW Hirondelle flank have a minimum age of 1.55 Ma (Storch et al., 2020). D. João de Castro volcano is still active as evident from seismic activity, hydrothermal venting (Cardigos et al., 2005), and the latest recorded eruption occurred 1720 CE reaching subaerial levels but was later eroded to a water depth of ∼12 m below sea level (mbsl) (Weston, 1964).

3. Sampling and Methods

3.1. Bathymetry and Sampling

Bathymetric data from D. João de Castro seamount and its surrounding seafloor in the Hirondelle Basin were acquired during R/V Meteor cruises M113 (Hübscher et al., 2016) and M128 (Beier et al., 2017). The bathymetric data were obtained using the hull-mounted EM122 and EM710 multibeam systems with signal frequencies of 12 kHz and 70–100 kHz, respectively. The bathymetric data have a resolution of ∼20–40 m. Mapping of fault scarps and volcanic structures and the quantification of their orientations (Figure 2) was based on the bathymetric data using a local UTM projection (UTM zone 26N). Thus, the orientation data is a conformal projection of the working area. The geological mapping of the working area (Figure 3) is based on topographic differences and related structures from the bathymetry. The classification of units is, thus, not based on simple lithological variations (Figures 1c and S1; Table S1), but as interpreted from structural surface features and in part seismic profiles.

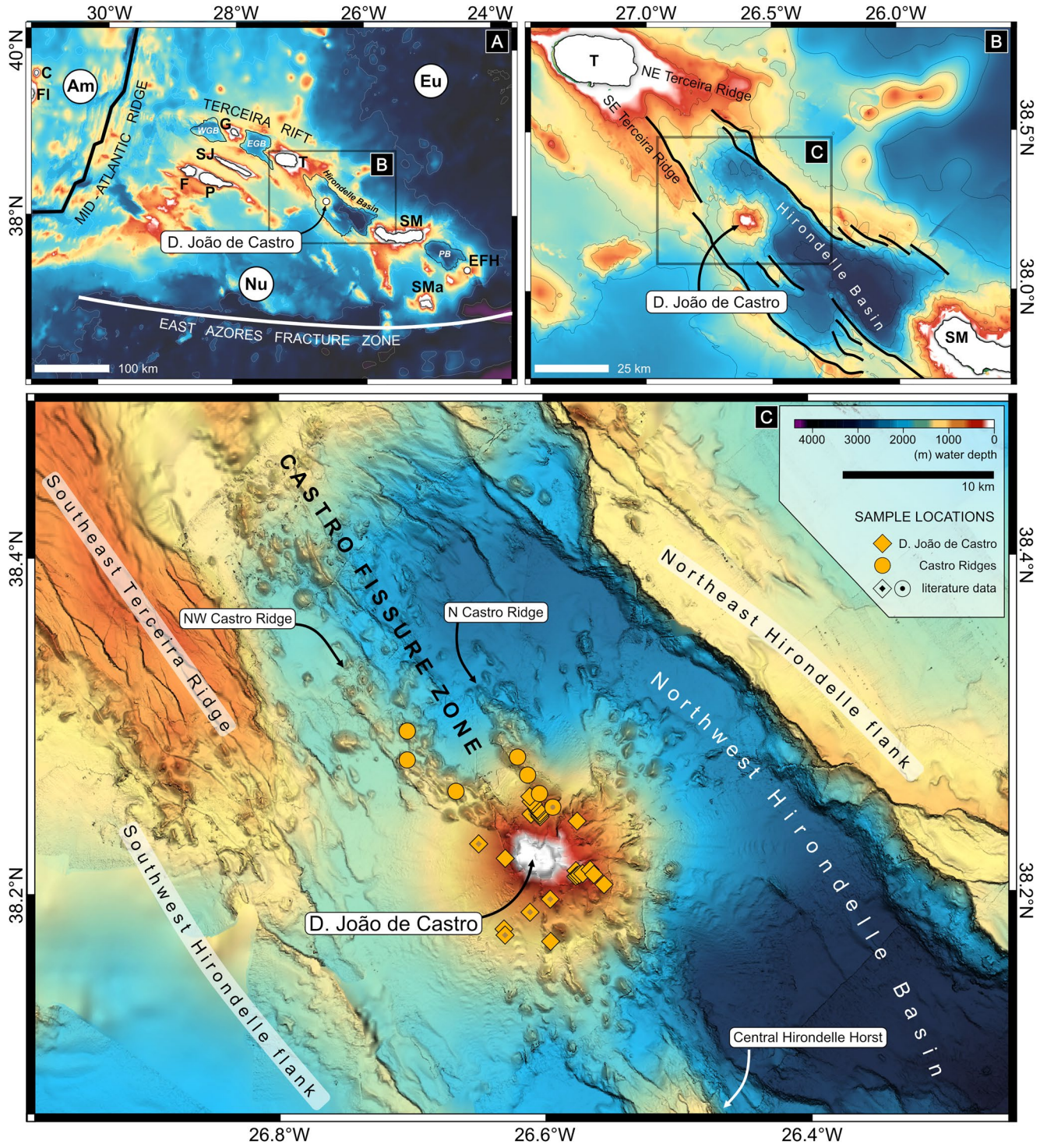

Figure 1. (a) Bathymetric map of the Azores Plateau with major tectonic boundaries. Volcanic islands, seamounts, and tectonic plates are abbreviated as follows: Graciosa (G), Terceira (T), São Miguel (SM), East Formigas High (EFH), São Jorge (SJ), Faial (F), Pico (P), Corvo (C), and Flores (F); Basins along the Terceira Rift: West Graciosa Basin (WGB), East Graciosa Basin (EGB), and Povoação Basin (PB); Tectonic plates: North-American Plate (Am), Eurasian Plate (Eu), Nubian Plate (Nu). Bathymetric maps of (b) the Hirondelle Basin and adjacent magmatic centers along the Terceira Rift axis; and (c) the D. João de Castro seamount in the NW Hirondelle Basin. In (b) thick black lines highlight the basin margin faults of the Hirondelle Basin. Note that in the SE Hirondelle Basin these faults form left-stepping transfer zones as result of basin segmentation. In (c) symbols highlight locations of volcanic rocks obtained during R/V Meteor cruises M113 (Hübscher et al., 2016) and M128 (Beier et al., 2017). Sample locations for literature data are from cruises Pos232 and Pos286 with R/V Poseidon (Beier et al., 2008).

10.1029/2020TC006663

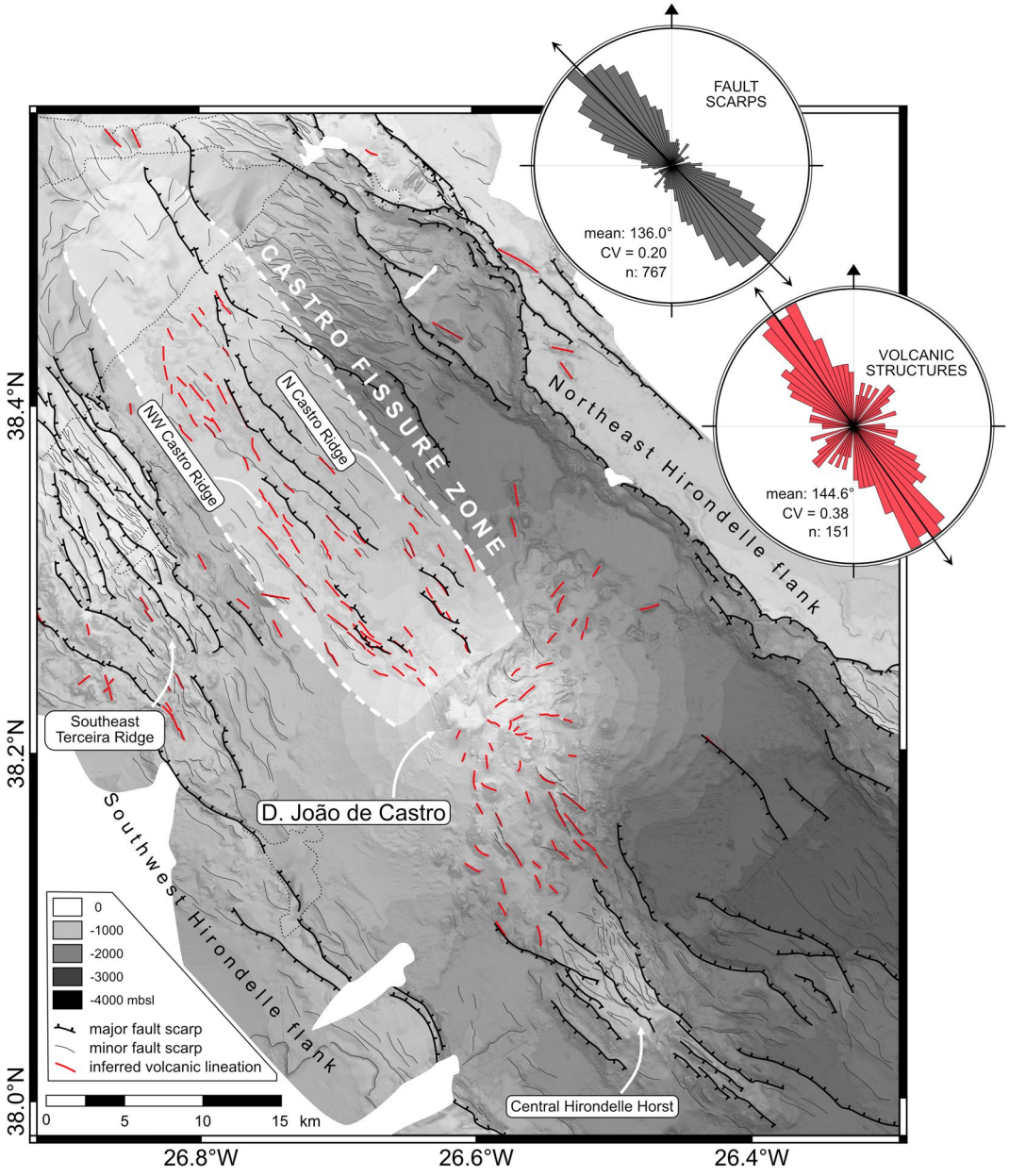

Figure 2. Structural map of the D. João de Castro seamount in the NW Hirondelle Basin. Black and red lines indicate fault scarps and volcanic structures with a preferred orientation obtained from the bathymetry. Insets show rose diagrams (area proportional to frequency; Nemec, 1988) of strike directions of fault scarps (gray) and volcanic structures (red) of the entire shown area. The mean strike directions, the circular variances (CV) and the number of tectonic or volcanic lineaments (*n*) are indicated. White field with dashed line highlights the focused occurrence of volcanic features in the NW Hirondelle Basin that are summarized as the Castro Fissure Zone.

Submarine rock samples and volcanic glasses from D. João de Castro were taken from the uppermost flanks at ~300–1,350 mbsl at the NW and N Castro Ridges (Figure 1c). We grouped the samples from the D. João de Castro magmatic system based on whether they derive from the main edifice or the Castro Ridges, respectively. Samples were taken by TV-guided grab (GEOMAR Helmholtz-Zentrum für Ozeanforschung) and with a Remotely Operated Vehicle (ROV MARUM Quest 4000). Literature data used here (Béguelin et al., 2017; Beier et al., 2008) are from dredge sample locations at the flanks of the edifice.

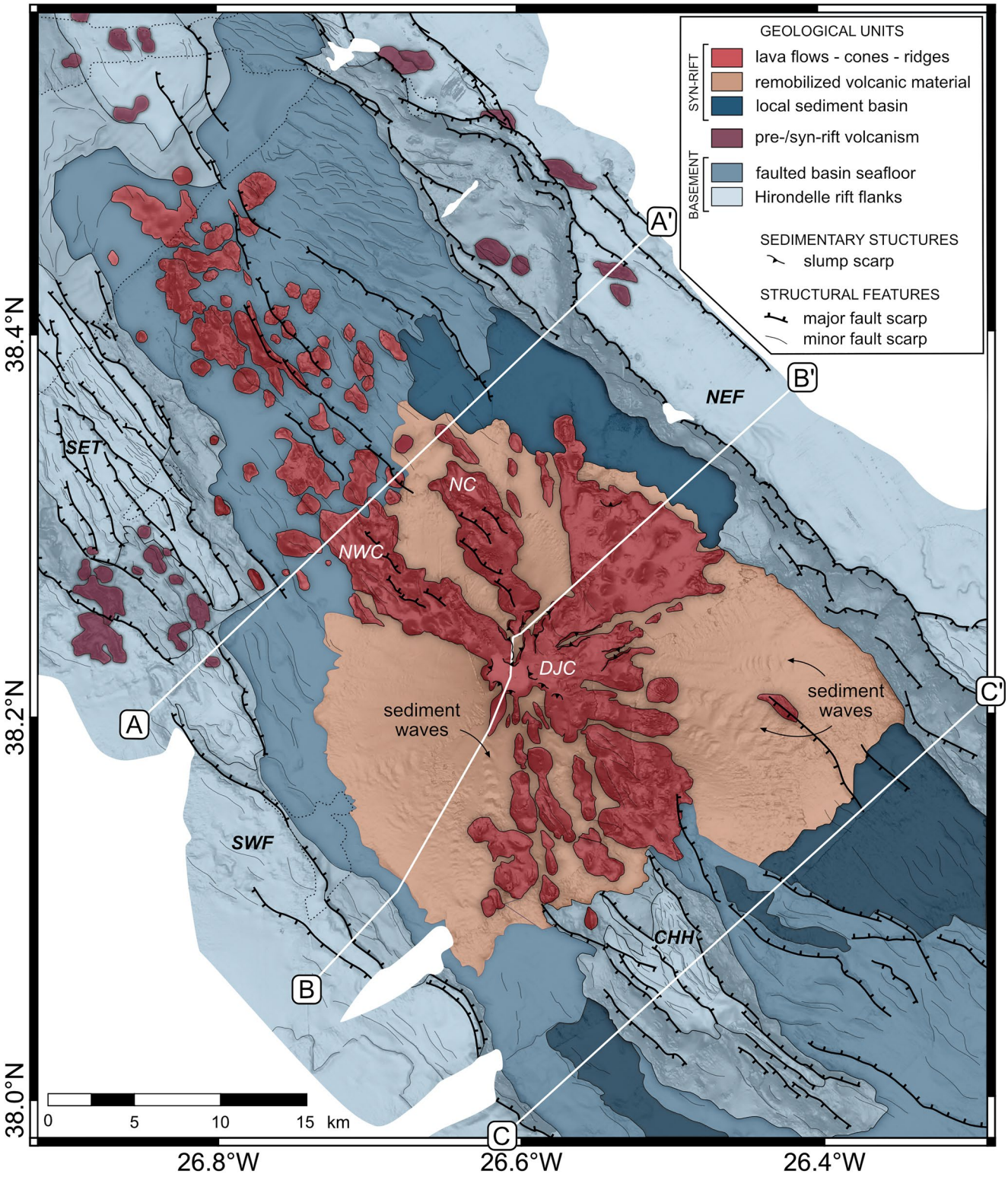

Figure 3. Geological map of the D. João de Castro seamount in the NW Hirondelle Basin. Geological units are distinguished based on bathymetric surface features, rocks samples from the D. João de Castro seamount and the Castro Ridges (see Figure 1) and seismic imagery. "Remobilized volcanic material" consists of volcanic debris and talus as well as reworked volcanic units due to rotational slumping. Lines A-A′, B-B′ and C-C′ are seismic profile lines across different areas of the NW Hirondelle Basin shown in Figure 4. Volcanic units are indicated with abbreviations: D. João de Castro (DJC), N Castro Ridge (NC), NW Castro Ridge (NWC), NE Hirondelle flank (NEF), SW Hirondelle flank (SWF), SE Terceira Ridge (SET), and Central Hirondelle Horst (CHH).

3.2. Seismic Imagery

Three seismic profiles in the NW Hirondelle Basin were obtained, crossing the D. João de Castro edifice as well as across the regions to its northwest and southeast, respectively (Figures 3 and 4). The seismic profile lines were obtained during R/V Meteor expedition M113 (Hübscher et al., 2016). Seismic signals were generated using an array of three GI-Guns and one Mini-Gun in a water depth of about 2.5 m. The streamer used was a digital 144-channel streamer of 600 m active length. Data processing included frequency filtering (15–350 Hz), gain, velocity analysis (every 50 CMPs), NMO-correction, coherency filtering, time migration, bandpass, white noise removal, dip filtering, and fx deconvolution. The profile across D. João de Castro is stacked from individual profiles accordingly in order to receive a line closest to a transect perpendicular relative to the Hirondelle flanks. For a detailed overview of the method see Hübscher and Gohl (2014).

3.3. Geochemical Methods

Major element analyses for whole rocks from cruises M113 and M128 were carried out using a Spectro XEPOS He - XRF spectrometer at the GeoZentrum Nordbayern (GZN), Friedrich-Alexander-Universität (FAU) Erlangen-Nürnberg following the methods described in Romer et al. (2018). Precision and accuracy are better than 0.8% (2σ) and 1% (2σ), respectively, based on repeated measurements of the international rock standard BE-N, BR, and BHVO-1 (Tables S1/S2).

The major element analyses of glasses were performed on a JEOL JXA-8200 Superprobe electron microprobe at the GZN, FAU Erlangen-Nürnberg using methods and standards described in Beier, Brandl, et al. (2018). An acceleration voltage of 15 kV, a beam current of 15 nA, and a defocused beam (10 μm) were used. Precision and accuracy relative to the natural volcanic glass standards VG A-99 were better than 5% (2σ) (Beier, Brandl, et al., 2018; Brandl et al., 2012).

Solution trace element analyses for selected submarine whole-rock samples were carried out using a Thermo Fisher Scientific X-Series 2 quadrupole ICP-MS connected to an Aridus 2 membrane desolvating sample introduction system at the GZN, FAU Erlangen-Nürnberg. For the dissolution of sample powder and rock standards (BHVO-2), we used the method described in detail in Freund et al. (2013), following standard techniques using a 3:1 mixture of HF and HNO_3. Precision and accuracy are better than 1.1% (2σ) and 1.1% (2σ), respectively, based on repeated measurements of the international rock standard BHVO-2.

Strontium-Nd-Pb isotope data from submarine samples from D. João de Castro were processed and analyzed at the GZN, FAU Erlangen-Nürnberg. For Sr-Nd-Pb analysis, ~150–200 mg dried sample powder and glasses were leached in hot 6M HCl for at least 2 h and in a 1:1:2 mixture of H_2O_2, 2.5M HCl, and Milli-Q H_2O, respectively, then dissolved using the method described in Haase et al. (2017). Strontium and Nd were separated in ion-exchange columns using Biorad 50W-X8 (200–400 mesh) cationic resin with variably concentrated HCl. Neodymium was separated from Sm using LN-spec resin and the method described in Haase et al. (2017).

Strontium and Nd isotopes were analyzed using a Thermo Fischer Triton Plus thermal ionization multicollector mass spectrometer in static mode. Strontium isotope measurements were corrected for mass fractionation using $^{88}Sr/^{86}Sr = 0.1194$, and mass 85 monitored to correct for a possible contribution of ^{87}Rb to mass 87. Neodymium isotope data were corrected for mass fractionation using a $^{146}Nd/^{144}Nd$ ratio of 0.7219. Samarium interference on masses 144, 148, and 150 was corrected by measuring ^{147}Sm, although the correction was negligible for all samples presented here. During the analysis, SRM987 standard yielded $^{87}Sr/^{86}Sr = 0.710256 \pm 0.000005$, and the Erlangen Nd standard gave $^{143}Nd/^{144}Nd = 0.511543 \pm 0.000003$ (corresponding to a value of 0.511850 for the La Jolla Nd isotope standard). The data were not normalized to the measured standards.

For the digestions and Pb column chemistry, only double-distilled acids were used to keep the blanks as low as possible. The separation of Pb was carried out using the method detailly described in Romer et al. (2018) using Sr-spec resin column chemistry. Lead isotope measurements were carried out on a Thermo Fisher Neptune MC-ICP-MS using a $^{207}Pb/^{204}Pb$ double spike to correct for instrumental mass fractionation. Spiked and unspiked sample solutions were introduced into the plasma via a Cetac Aridus desolvating nebulizer and measured in static mode. Interference of ^{204}Hg on mass 204 was corrected by monitoring ^{202}Hg. An

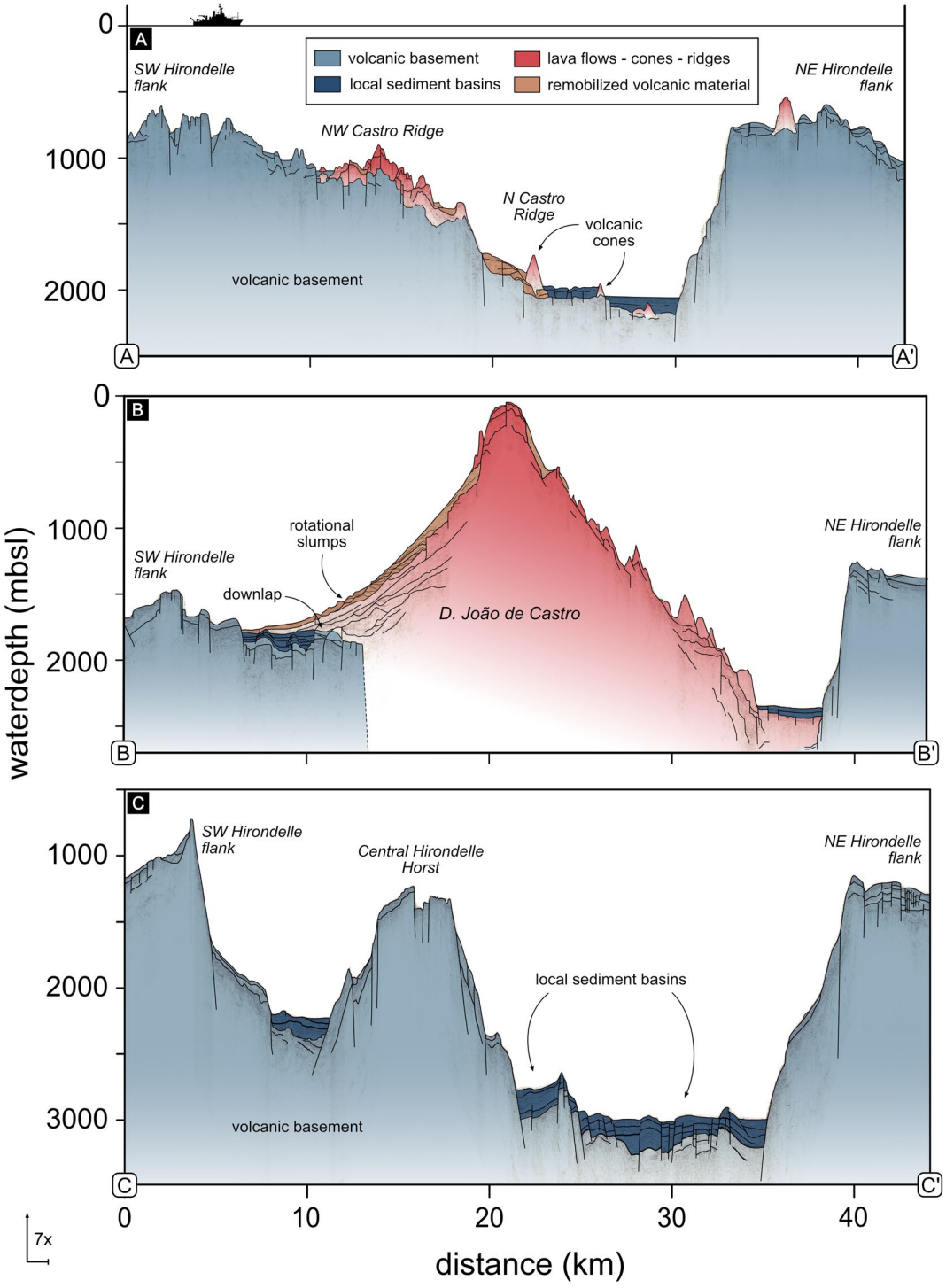

Figure 4. Seismic profile lines across the NW Hirondelle Basin showing the Hirondelle Basin flanks and the basin interior as highlighted in Figure 3. Characteristic features of the profiles are (a) the N and NW Castro Ridges, (b) the D. João de Castro volcano, and (c) the Central Hirondelle Horst. The geological units are the same as defined in Figure 3. Profiles are seven-times vertically exaggerated.

exponential mass fractionation correction was applied offline using the iterative method of Compston and Oversby (1969), the correction was typically 4.5‰ per amu. Twenty measurements of the NBS981 Pb isotope standard (measured as an unknown) throughout this study gave $^{206}Pb/^{204}Pb$, $^{207}Pb/^{204}Pb$, and $^{208}Pb/^{204}Pb$ ratios of 16.9415 ± 0.0004, 15.4992 ± 0.0006, and 36.7243 ± 0.0017, respectively. The Pb blanks are generally below 30 pg.

4. Geology of the Northwest Hirondelle Basin

4.1. Bathymetry of the Hirondelle Basin

The Hirondelle Basin is the largest of four submarine rift basins along the Terceira Rift (Figure 1a). It is located between the islands Terceira in the northwest and São Miguel in the southeast (Figure 1b). The Hirondelle Basin extends for 120 km in an NW-SE elongation and has a width ranging from 25 to 40 km. The seafloor of the rift basin is between 300 and 2,000 m lower than the surrounding rift flanks, whereas the deepest area is located in the southeast, with a maximum water depth of ~3,200 mbsl. The rift flanks of the Hirondelle Basin are not continuous NW-SE structures, indicating that the basin is segmented (Figure 1b). At ~26.0°W, 38.0°N the SW and NE Hirondelle flanks display a lateral offset along an SW-NE line of ~15 km with left-stepping transfer zones.

The northwestern part of the Hirondelle Basin is dominated by the D. João de Castro seamount and related structural and volcanic features. D. João de Castro is a subcircular, solitary volcanic edifice comparable to some central volcanoes from the Azorean islands, for example, Pico on Pico Island. The edifice has a radius of ~13 km and a height of ~2,500 m relative to the seafloor at its northeastern flank. The top of the volcano is presently at ~12 mbsl (Figure 1c). The D. João de Castro seamount is a large volcanic edifice representing a magmatic center in the otherwise amagmatic or magma deficient Hirondelle Basin (Figure 1). It is situated in the center of the 30–35 km wide rift basin, bordered by the uplifted NE and SW Hirondelle flanks, the SE Terceira Ridge (NW), and the foothills of the Central Hirondelle Horst (SE). The maximum water depth of the seafloor at the southwestern flank of D. João de Castro is ~1,600 mbsl, notably lower compared to the northeastern and eastern flanks at ~2,500 and ~3,000 mbsl water depth. Similarly, the SW Hirondelle flank is less pronounced with ~350 m vertical difference relative to the neighboring seafloor compared to the NE Hirondelle flank with ~1,200 m.

4.2. Fault Scarps and Basin Geometry

D. João de Castro and the Hirondelle basin flanks formed from different volcanic eruptions covering some 0.46 Ma (Storch et al., 2020) affected by different regional tectonic stresses. This resulted in a diverse range of volcanic units and structural features of different vertical offset, dip, and orientation. The NE Hirondelle flank at D. João de Castro is formed by a well-defined steep border fault with the highest vertical offset in the NW Hirondelle Basin (Figure 2). In several places, the NE Hirondelle flank branches into subsidiary faults to form relay ramps, for example, north of D. João de Castro (Figures 1c and 2). In contrast, the SW Hirondelle flank at D. João de Castro has a diffuse faulting pattern over a broader zone of up to 20 km width, gradually increasing in water depth from the flank's top into the faulted basin seafloor. The majority of fault scarps at the SW Hirondelle flank and, in particular, the SE Terceira Ridge are dipping toward the SW. The NE-dipping fault scarps, however, form the basin margin faults of the Hirondelle Basin with 100–200 m vertical offsets. Further fault scarps dipping toward the northeast are situated in the interior of the Hirondelle Basin, in particular at the N and NW Castro Ridges and the northwestern continuation. Here, NE-dipping fault scarps are more abundant compared to SW-dipping faults but individually have smaller vertical offsets of 100–300 m, comparable to the SW Hirondelle flank. In contrast, the SW-dipping fault scarps at the NE Hirondelle flank NE of D. João de Castro have higher offsets of up to 1,200 m. This pattern results in an asymmetric, staircase-like geometry of the seafloor, where the NE Hirondelle flank is steeper compared to the SW Hirondelle flank. The difference in water depth between, for example, SW and NE across the N Castro Ridge is up to 400 m at a lateral distance of 4 km showing that the faults coincide with the volcanic structures (Figure 2). This system of fault scarps at and northwest of the Castro Ridges together with extensive normal faulting at the Central Hirondelle Horst (Figure 2) forms an NW-SE-striking band of northeast dipping normal faults.

The orientation of fault scarps in the northwestern part of the Hirondelle Basin have a mean NW-SE strike direction (mean: 136°) and a comparably low circular variance of 0.20 (Figure 2). Our data are comparable to the structural analyses of Casalbore et al. (2015) on the fault scarps at the SE Terceira Ridge striking between 112° and 163° with a frequency maximum at ~140°. Fault scarps at the main volcanic structure of D. João de Castro are less abundant but display a similar general NW-SE orientation. Additionally, several amphitheater-shaped head scarps are concentrated at the top of the edifice (Figure 3), which is a common geomorphological feature during the evolution of volcanic edifices and seamounts reflecting local volcano instabilities and gravitational failures (Delcamp et al., 2018; Karátson et al., 1999; Mitchell & Lofi, 2008). Groups of parallel trending and opposingly dipping scarps being distributed radially around the volcano's summit and flanks indicate the presence of distinct sediment pathways such as gullies and channels (Figure 3). These are associated with erosive processes, for example, turbiditic downslope material transport, rather than constructive volcanic processes that lead to the formation volcanic ridges, cones, and lava flows (Tempera et al., 2013).

4.3. Basin Morphology and Volcanic Structures

Unfaulted and intact, and faulted volcanic cones occur both within the Hirondelle basin and on the flanks (Figures 2 and 3), respectively. In the basin, these are located either at D. João de Castro along the volcanic ridges or as solitarily cones on faulted sections of the seafloor. We interpret the volcanic formations in the center of the actively rifting Hirondelle Basin to be the result of syn-rift volcanism. Seismic profiles A-A′ and B-B′ across the main edifice and the Castro Ridges display that these volcanic formations are located on top of the rifted volcanic basement (Figures 4a and 4b). Volcanic cones on top of the rift flanks could be of pre-rift and/or syn-rift origin, considering that the Terceira Rift is active. The basin seafloor around D. João de Castro is strongly faulted and forms an irregular, rough topography. In contrast, some areas are dominated by a flat, smooth, and less-faulted surface. Particularly, the seafloor at the base of NE Hirondelle flank is notably deeper than its surroundings and forms the sediment depocenter in this section of the basin indicating higher subsidence rates compared to the seafloor at the SW flanks (Figures 3 and 4c). In the interpreted seismic profiles, sediment fillings occur as faulted (Figure 4c) and non-faulted layered strata (Figure 4a), whereas non-faulted sedimentary deposits occur exclusively on top of syn-rift volcanic units north and northwest of D. João de Castro.

The D. João de Castro seamount consists of the main volcanic edifice and a series of volcanic cones situated along its flanks that commonly occur in alignments along with volcanic ridges (Figures 2 and 3). Two parallel volcanic ridges extend from the northern (N Castro Ridge) and northwestern (NW Castro Ridge) flanks of D. João de Castro in a northwestern direction (Figures 3 and 4a). These features are comparable to the submarine and subaerial volcanic ridges that extend from many of the Azores islands, for example, the Serreta Ridge (Terceira; Chiocci et al., 2013), the Capelo Fissure Zone, the Capelinhos rift (Faial, Romer et al., 2018; Trippanera et al., 2014), and the western part of Sete Cidades volcano (São Miguel; Weiß, Hübscher, Wolf, et al., 2015), as well as those observed at other ocean islands, for example, Fernandina Island (Galápagos; Geist et al., 2006). The N and NW Castro Ridges extend from the volcano's center ~10 and 15 km into the rift basin, respectively (Figure 3). Single and alignments of cones and narrow, symmetric ridges adjoin the volcanic ridges in the northwest forming a ~35 km long and ~8 km wide volcanically active zone extending from D. João de Castro's center into the rift basin (Castro Fissure Zone, Figure 2). Numerous large volcanic cones and lava domes straddle the flanks of D. João de Castro seamount corresponding to parasitic volcanic vents on the flanks of the central volcano.

The western, southwestern, and eastern flanks of D. João de Castro are dominated by fan-shaped deposits, with a much smoother topography compared to the rougher areas dominated by volcanic ridges and cones (Figure 3). The units with a smooth topography occur close to the volcano's top as narrow fillings in the radiating gullies and channels and become broader along the flank and the base of the edifice. The volcanic fan at the southwestern flank reaches a total width of ~15 km at the base. Despite their large size and the high-resolution bathymetry, these fans cannot be easily subdivided into single units, for example, individual debris flows. All fans along the flanks of D. João de Castro display downstream sediment wave structures of 0.5–3 km width and ~50–100 m height in the overall smooth topography (Figure 3). These most commonly occur along continental margins (e.g., Nelson et al., 2000) but also along the flanks of ocean island

associated with either eruption-fed supercritical density flows (turbidity currents) or rotational landslides (Pope et al., 2018). Seismic imagery on the southwestern flank of D. João de Castro reveals sequences of layered volcanic strata extending from the edifice's top toward its flanks. The uppermost layers display remobilization of volcanic material at D. João de Castro, partly due to rotational slumping (Figure 4b).

The majority of volcanic features in the NW Hirondelle Basin have a preferred orientation either by the alignment of volcanic cones or elongated ridges of variable size. Quantitative mapping of these volcanic structures yields a mean NW-SE strike direction (mean: 144.6°, Figure 2) with a comparably high circular variance of 0.38. Thus, the mean orientation of volcanic structures is comparable to the orientation of fault scarps in the same area. The orientation of volcanic structures in the NW Hirondelle Basin is also similar compared to those observed in the neighboring volcanic systems, that is, the western part of São Miguel (Carmo et al., 2015) and its submarine volcanic ridges (Weiß, Hübscher, & Lüdmann, 2015) and the NW Terceira Ridge offshore Terceira Island (Casalbore et al., 2015) all of which are striking NW-SE. The N and NW Castro Ridges are the most pronounced volcanic structures at D. João de Castro that have NW-SE oriented volcanic structures. There is no systematic difference between the orientation of volcanic structures at the Hirondelle Basin rift flanks and within the basin along the ridges. However, other volcanic features at the flanks of D. João de Castro are often oriented contrasting the mean strike direction (striking between 5° and 110°) without forming a second frequency maximum (Figure 2). Instead, they form a subordinate circumferential azimuthal distribution around the edifice's center. These contrasting structural features are limited to the flanks of the seamount within a radius of ~15 km from the center. A seismic profile (C-C′) across the Central Hirondelle Horst (Figure 4c) reveals that syn-rift volcanism is absent southeast of D. João de Castro and predominantly occurs in a northwesterly direction (Figures 2 and 3).

5. Geochemistry of D. João de Castro

5.1. Major and Trace Element Geochemistry

Lavas from D. João de Castro seamount and the Castro Ridges (Figure 1) cover the entire range from alkali basalts to trachytes (Figure 5a). Based on the TAS (total alkali vs. silica) classification from Le Maitre et al. (1989), few highly porphyritic lavas with MgO contents >12 wt. % are subalkaline basalts, whereas the majority of D. João de Castro lavas are lavas from the alkaline series (Figure 5a). Consistent with data from Beier et al. (2008), lavas from D. João de Castro range from ~17 wt. % to 0.9 wt. % MgO (Figure 5). The most primitive volcanic glass rim has a MgO content of 5.9 wt. %. Lavas exceeding ~12 wt. % MgO are highly olivine- and clinopyroxene-phyric and reflect the accumulation of clinopyroxene and olivine phenocrysts. The major element composition of lavas from D. João de Castro and the Castro Ridges lie on well-defined trend lines versus MgO contents. The variability of major element contents is comparable to those from São Miguel and Terceira, for example, ranging from 3 to 4 wt. % Na_2O and 8 to 12 wt. % CaO at a given MgO content of ~6 wt. %. Lavas from the D. João de Castro edifice and the Castro Ridges overlap, indicating no systematic differences except for their K_2O contents (Figure 5c). In terms of K_2O, a few Castro Ridge lavas are slightly lower, with 0.8–1.0 compared to 1.7–2.0 wt. % K_2O at 9–6 wt. % MgO, respectively.

Incompatible trace element ratios such as Nb/Zr display similar ranges compared to those from Terceira and São Miguel (Figure 6a). For MgO contents >5 wt. %, Nb/Zr ratios range from 0.18 to 0.25. There is no systematic difference in these ranges, depending on whether they derive from D. João de Castro or the Castro Ridges. Lavas from D. João de Castro have higher La/Yb and Tb/Yb ratios of ~18–25 and 0.42–0.50, respectively, than lavas from the Castro Ridges ranging from 12 to 19, and from 0.38 to 0.45 (at ~6 wt. % MgO), respectively (Figures 6b and 6c). The overall differences in Tb/Yb between the Castro Ridges and the central edifice are, however, subtle.

In agreement with observations made by Beier et al. (2008), the major and trace element patterns of the D. João de Castro, Terceira, and São Miguel magmatic systems display systematic differences. The TiO_2 contents of D. João de Castro lavas overlap with those from Terceira, both being generally lower compared to lavas from western São Miguel (Figure 5b). In contrast, the K_2O contents of D. João de Castro lavas overlap with those from western São Miguel, and both systems generally have higher K_2O contents compared to the Terceira lavas (Figure 5c). The La/Yb ratios of D. João de Castro overlap with São Miguel, whereas lavas

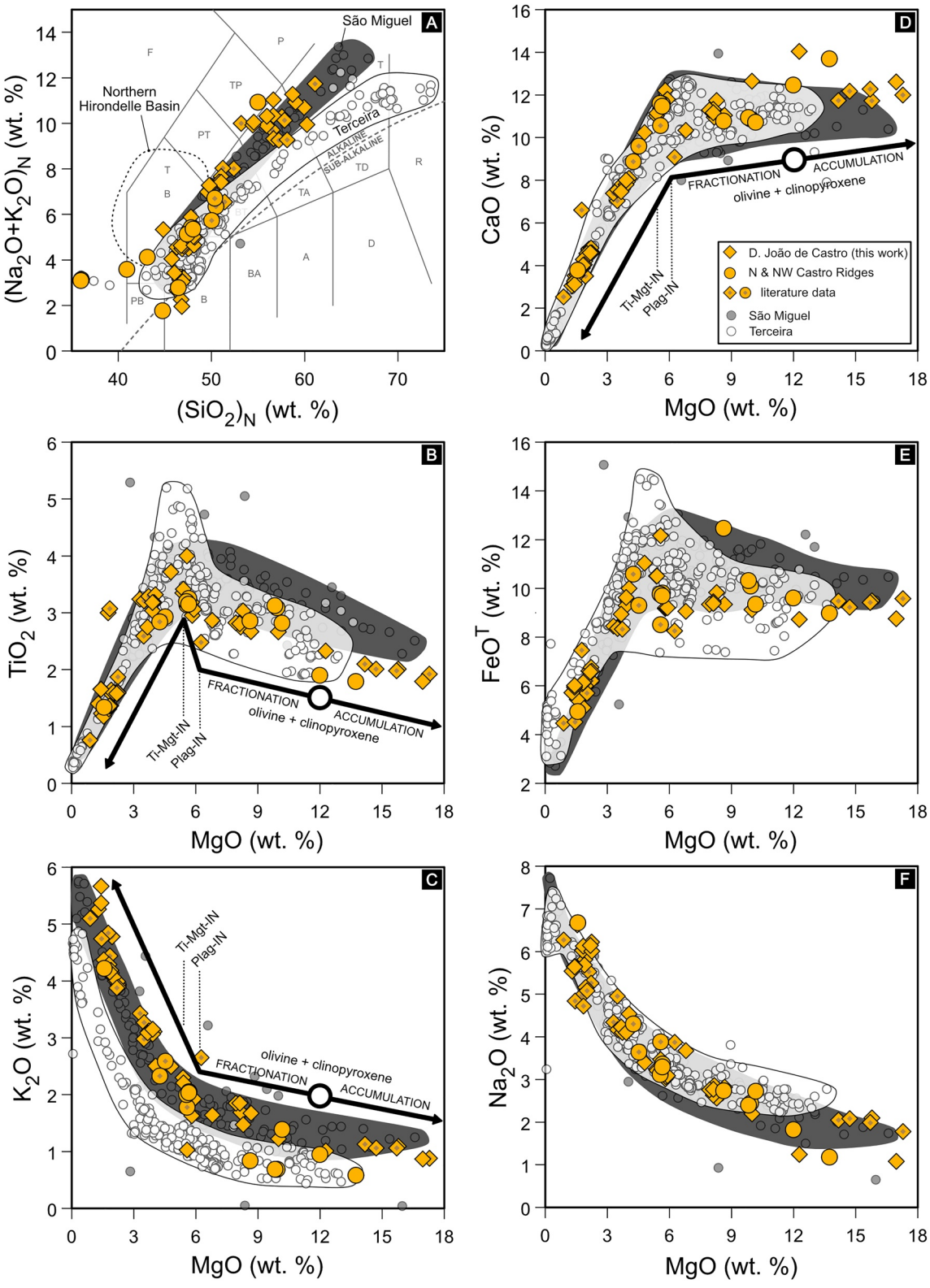
A
São Miguel
Northern Hirondelle Basin
Terceira
ALKALINE
SUB-ALKALINE
F
P
T
TP
PT
T
B
TD
R
TA
D
BA
A
PB
B
$(Na_2O+K_2O)_N$ (wt. %)
$(SiO_2)_N$ (wt. %)
D
CaO (wt. %)
MgO (wt. %)
FRACTIONATION
ACCUMULATION
olivine + clinopyroxene
Ti-Mgt-IN
Plag-IN
D. João de Castro (this work)
N & NW Castro Ridges
literature data
São Miguel
Terceira
B
TiO_2 (wt. %)
MgO (wt. %)
FRACTIONATION
ACCUMULATION
olivine + clinopyroxene
Ti-Mgt-IN
Plag-IN
E
FeO^T (wt. %)
MgO (wt. %)
C
K_2O (wt. %)
MgO (wt. %)
Ti-Mgt-IN
Plag-IN
olivine + clinopyroxene
FRACTIONATION
ACCUMULATION
F
Na_2O (wt. %)
MgO (wt. %)

Figure 5

from the Castro Ridges have as low La/Yb ratios as Terceira. The Tb/Yb ratios of lavas from D. João de Castro generally overlap with Terceira lavas and are lower than those from São Miguel (Figures 6b and 6c).

5.2. Isotope Geochemistry

Lavas from the D. João de Castro magmatic system cover a wide range in Sr-Nd-Pb isotope space. They lie on a mixing line between the "common Azores" mantle endmember with a Pb isotope composition of $^{206}Pb/^{204}Pb$ ~19.5, $^{207}Pb/^{204}Pb$ ~15.62, and $^{208}Pb/^{204}Pb$ of ~39.2 (Béguelin et al., 2017; Beier, Haase, et al., 2018, Figures 6e and 6f) and the mantle endmember specific to D. João de Castro which has comparably unradiogenic Pb isotope ratios. Similarly, the Sr-Nd isotope space describes a broad field, where several Azores magmatic systems form mixing lines between individual sources and the common Azores mantle source (Figures 6d and 6e). For systems along the Terceira Rift this endmember has $^{87}Sr/^{86}Sr$ ratios around ~0.7035 and $^{143}Nd/^{144}Nd$ ratios between 0.5129 and 0.5130 (Beier et al., 2008). In the case of D. João de Castro this source mixes with a low $^{143}Nd/^{144}Nd$ but only slightly more radiogenic $^{87}Sr/^{86}Sr$ of ~0.7037 endmember (Figure 6d). New data from the central seamount and the Castro Ridges overlap with existing data from Beier et al. (2008) but significantly increase the isotopic range of the D. João de Castro magmatic system toward both enriched and depleted compositions, particularly in Pb isotope space, that is, ranging from ~18.6 to 19.6 and from ~38.4 to 39.2 for $^{206}Pb/^{204}Pb$ and $^{208}Pb/^{204}Pb$, respectively (Figures 6e and 6f). The $^{143}Nd/^{144}Nd$ isotope ratio of the D. João de Castro endmember is <0.5128 and defines a binary mixing trend with an Azores-typical endmember of $^{143}Nd/^{144}Nd = 0.5129$ (except for two outlier samples [IEAZO0898, IEAZO0923]; Figure 6e). In agreement with observations made based on source sensitive trace element ratios, the isotopic signature of lavas from the Castro Ridges and the central edifice overlap.

The D. João de Castro magmatic system thus has a distinct, well-defined mantle source signature like other magmatic systems along the Terceira Rift and the eastern Azores (Beier et al., 2008). The neighboring islands of São Miguel and Terceira as well as other magmatic systems along the Terceira Rift, for example, Graciosa and lavas from the Northern Hirondelle Basin, are isotopically extremely variable and distinct from D. João de Castro (Beier, Haase, et al., 2018; Storch et al., 2020). The differences in major and trace elements and Sr-Nd-Pb isotopes at D. João de Castro and the variability observed in the neighboring magmatic system indicate a systematic variability of mantle sources and the melting conditions along the Terceira Rift and the eastern Azores Plateau.

6. Discussion

Volcanoes forming in active rift systems are the manifestation of the interaction of magmatic and tectonic processes. The composition of the erupted lavas reflects the composition of the mantle sources as well as the melting and melt extraction processes and magma evolution. The morphology of the volcanic edifice reflects the lithospheric stress regime and also the vertical and horizontal transport of magma through the crust. The spatial distribution of structural features related to tectonic stresses and volcanic processes allows reconstructing how volcanic rift systems evolve in time and space.

6.1. The Distribution of Tectonic and Volcanic Structures in the Northwest Hirondelle Basin

The consistent NW-SE strike direction of fault scarps in the NW Hirondelle Basin (Figure 2) shows that this region has been dominated by a single regional tectonic stress field since the opening of the basin. The movement of the Nubian and Eurasia Plates and the opening of the Hirondelle Basin results from an extensional movement in northeastern and southwestern directions (Marques et al., 2013). This is consistent

Figure 5. (a) Total Alkali versus SiO_2 (TAS) classification of Le Maitre et al. (1989). Dashed line separates the alkaline from the sub-alkaline volcanic series (after Irvine & Baragar, 1971). (b) TiO_2, (c) FeO^T, (d) CaO, (e) Na_2O, and (f) K_2O versus MgO contents for lavas from D. João de Castro volcano and the N and NW Castro Ridge. Literature data show lavas from the adjacent magmatic systems Terceira (Beier et al., 2008; Hildenbrand et al., 2014; Madureira et al., 2011; Pimentel et al., 2016; Romer et al., 2019; Self, 1976; Zanon & Pimentel, 2015), São Miguel (Beier et al., 2006; Elliott et al., 2007; Haase & Beier, 2003; Turner et al., 1997; Widom et al., 1997; Zanon, 2015), and the Northern Hirondelle Basin flank (Storch et al., 2020). Literature data from D. João de Castro from Beier et al. (2008). Arrows in (b–d) show generalized liquid lines of descent typical for ocean island basalts (modified from Prytulak & Elliott, 2007).

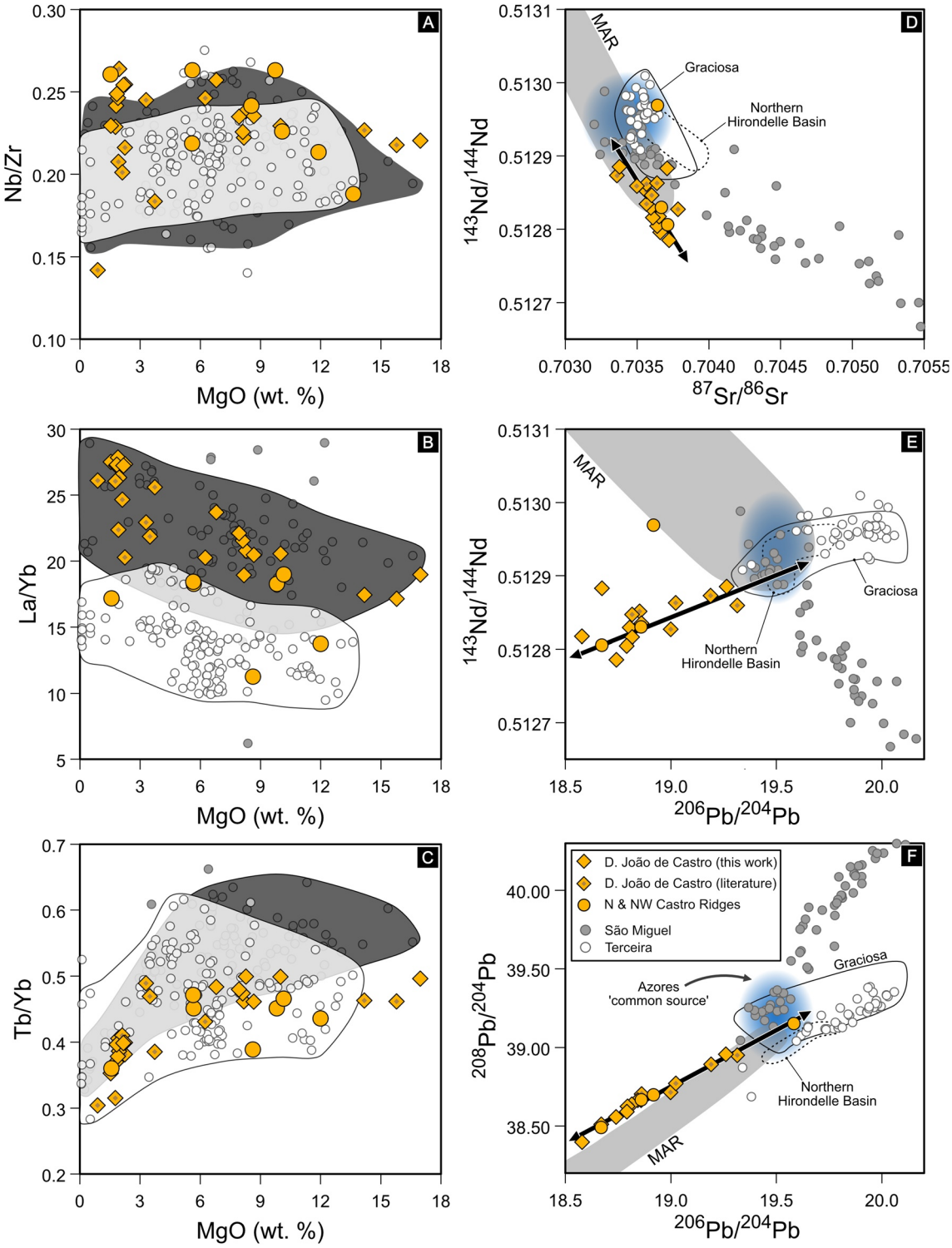
A
Nb/Zr
MgO (wt. %)
B
La/Yb
MgO (wt. %)
C
Tb/Yb
MgO (wt. %)
D
MAR
Graciosa
Northern Hirondelle Basin
$^{143}Nd/^{144}Nd$
$^{87}Sr/^{86}Sr$
E
MAR
Graciosa
Northern Hirondelle Basin
$^{143}Nd/^{144}Nd$
$^{206}Pb/^{204}Pb$
F
D. João de Castro (this work)
D. João de Castro (literature)
N & NW Castro Ridges
São Miguel
Terceira
Azores 'common source'
Graciosa
Northern Hirondelle Basin
MAR
$^{208}Pb/^{204}Pb$
$^{206}Pb/^{204}Pb$

Figure 6

with previous structural studies on this section of the Terceira Rift, that is, the SE Hirondelle Basin (Weiß, Hübscher, & Lüdmann, 2015), the western part of São Miguel (Beier et al., 2006) at Terceira's eastern volcanoes (Madeira et al., 2015), and the offshore continuations at the NW and SE Terceira Ridges (Casalbore et al., 2015).

The dominant NW-SE orientation of volcanic structures in the NW Hirondelle Basin is comparable to the strike direction of the fault scarps (Figure 2). This implies that the lithospheric extension along the Terceira Rift is the dominant process controlling the shape and arrangement of volcanic structures, forming fault scarps and finally resulting in the opening of the Hirondelle Basin. It is commonly observed that tectonic stresses are a significant factor controlling the volcano's morphology. This is the case, both on large scales, for example, the alignments of central volcanoes in continental rift systems (Ebinger et al., 1999) or on a smaller scale within a single volcanic edifice, for example, oriented dike swarms at the Krafla volcanic system on Iceland associated with the extension along the MAR (Gudmundsson, 1987, 1998). The injection of dikes commonly occurs perpendicular to the maximum extensional stress σ_3 (Walker, 1999), that is, along a NW-SE strike direction in the Hirondelle Basin area of the Terceira Rift. Thus, the elongated alignment of volcanic cones and the formation of volcanic ridges in the NW Hirondelle Basin are the results of the emplacement of volcanic dikes in the framework of the regional tectonic stress field.

The concentration of volcanic activity along the Castro Fissure Zone, northwest of D. João de Castro is associated with the presence of normal faults with a large vertical offset (100–300 m) located in the center of the basin (Figures 2 and 4a). Profile A-A′ across the Hirondelle Basin shows that the SW Castro Ridge volcanism is located at boundaries between vertical topographic offsets of the faulted basin seafloor (Figure 4a). In contrast, seismic profile C-C′ (Figure 4c) and other seismic studies on the southeastern part of the Hirondelle Basin indicate amagmatic rifting of the volcanic basement with no evidence for syn-rift volcanism (Weiß, Hübscher, & Lüdmann, 2015). These areas are characterized by a negative free-air gravity anomaly relative to the surrounding seafloor, including the NW Hirondelle Basin (Vogt & Jung, 2004). Thus, the combined occurrence of large fault scarps and volcanism in the NW Hirondelle Basin is predominantly the result of the magmatism beneath D. João de Castro and the Castro Ridges (Figures 4a and 4b). The additional weakening of the lithosphere due to extensive diking events is thought to cause faulting and eruptions comparable to continental rift systems, for example, in the Main Ethiopian Rift (Corti, 2009; Kurz et al., 2007).

The circular azimuthal variance of the volcanic structures is significantly higher than those of the fault scarps (Figure 2). This shows that the syn-rift volcanic formations in the NW Hirondelle Basin have been influenced by an additional, albeit subordinate, process that has not visibly impacted on the formation of the fault scarps. Volcanic structures oriented differently from the mean NW-SE strike direction are controlled by a stress field in the crust that is different from the regional tectonic stress field. The distribution of these volcanic structures is radially around the D. João de Castro center (Figure 2) within a radius of ∼15 km. We interpret this to be a local subordinate stress field associated with the emplacement of the D. João de Castro edifice, generating circumferential extensional stresses (Acocella & Neri, 2009). These local stresses superimpose the regional tectonic stress field prevailing along this section of the Terceira Rift.

6.2. Mantle Source Heterogeneity

Volcanic activity along fissure zones is often directly linked with the magmatic activity at the central volcanic edifice. Several studies on volcanic systems, for example, on Iceland, have shown that fissure zones can

Figure 6. (a) Nb/Zr, (b) La/Yb, and (c) Tb/Yb trace element ratios versus MgO contents for lavas from D. João de Castro volcano and the N and NW Castro Ridge. Data sources are as in Figure 5. (d, e, f) Strontium-Nd-Pb isotope ratios of lavas from D. João de Castro volcano and the N and NW Castro Ridge along with literature data for lavas of other magmatic systems along the Terceira Rift, that is, Graciosa (Béguelin et al., 2017; Beier et al., 2008; Larrea et al., 2014), Terceira (Beier et al., 2008; Hildenbrand et al., 2014; Madureira et al., 2011; Romer et al., 2019), Northern Hirondelle Basin (Storch et al., 2020), and São Miguel (Beier et al., 2006; Elliott et al., 2007; Haase & Beier, 2003; Turner et al., 1997; Widom et al., 1997), and the MAR (Agranier et al., 2005; Dosso et al., 1999; Gale et al., 2011, 2013; Hamelin et al., 2013; Shirey et al., 1987). Literature data from D. João de Castro from Beier et al. (2008) and Béguelin et al. (2017). Blue fields in (e, f) highlight the area defined as "common Azores mantle" by Béguelin et al. (2017) and Beier et al. (2018). Blue field in (d) highlights typical Sr-Nd mantle endmember for volcanic systems along the Terceira Rift from Beier et al. (2008). Black arrows in (d, e, f) indicate possible mixing lines for the D. João de Castro lavas.

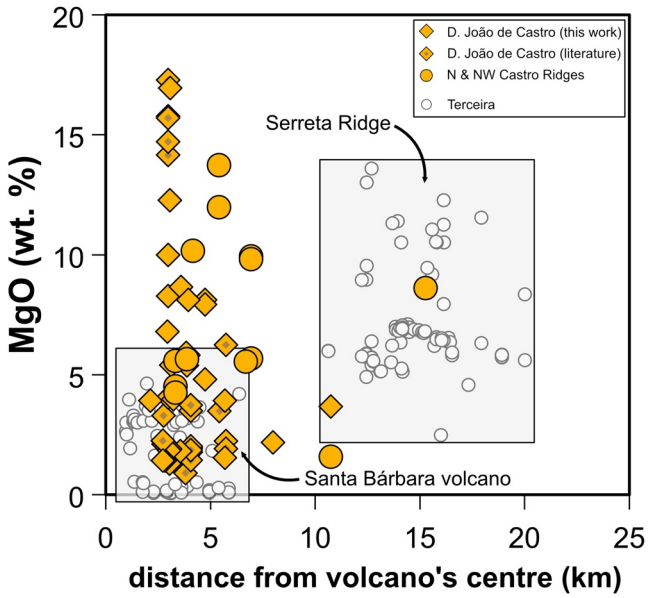

Figure 7. MgO contents versus the distance from the volcano's center of lavas from D. João de Castro volcano and the Castro Ridges along with literature data from the Santa Bárbara magmatic system consisting of the Santa Bárbara central volcano and the submarine Serreta Ridge. Data sources are as in Figure 5.

be fed from melt reservoirs situated beneath the central edifice by lateral melt transport via dikes (Sigurdsson & Sparks, 1978). The Castro Fissure Zone expands from the D. João de Castro seamount in a northwestern direction (Figure 1). Based on the distribution of volcanic and structural features and the focused volcanic activity at D. João de Castro and along the Castro Fissure Zone, we suggest that lavas from these localities form from the same mantle source. The geochemistry of these lavas allows disentangling the processes that lead to the formation of the central volcano and the fissure zone.

The Sr-Nd-Pb isotope ratios and source sensitive trace element ratios of lavas from D. João de Castro and the Castro Ridges are variable but cover a similar range and lie on a single mixing array for the entire system (Figure 6). This implies that both volcanic formations originated from the same mantle source, which is, however, highly heterogeneous like observed on other Azores volcanoes (Beier et al., 2007; Elliott et al., 2007; Turner et al., 1997; Widom et al., 1997). The eruption of lavas with distinct source isotopic signatures in a single magmatic system may be the result of episodic volcanic activity tapping discrete mantle sources. Episodic volcanic activity is well known from other magmatic systems in the Azores, for example, from the adjacent NW Hirondelle flank, where incompatible trace element and Nd-Hf isotope ratios of the lavas show distinct source compositions after a phase of volcanic quiescence of <90 ka (Storch et al., 2020). Lavas sampled at the N Castro Ridge and the eastern flank of D. João de Castro are fresh, glassy basaltic pillow lavas and submarine sheet flows, whereas lavas from the NW Castro Ridge display a higher degree of alteration with a higher proportion of volcanic breccias and sediments (Beier et al., 2017; Hübscher et al., 2016) (Figure S1). This could be indicative that these lavas are younger relative to those sampled from the NW Castro Ridge and possibly the SW flank of D. João de Castro, which would be consistent with an episodic volcanic activity; however, this remains speculative in the absence of radiometric ages.

Differences in La/Yb ratios between D. João de Castro and the Castro Ridges do not correlate with mantle source indicators (e.g., Sr-Nd-Pb isotopes, Nb/Zr) and are best explained by changes in the degree of melting. Lower La/Yb from the Castro Ridges suggest higher degrees of melting, while subtle differences in Tb/Yb imply similar amounts of residual garnet in the source and hence comparable melting depths (Bourdon et al., 2005, Figures 6b and 6c). In spite of similar variable source signatures, this implies that lavas from the Castro Ridges and at D. João de Castro are not all co-magmatic and either erupt at D. João de Castro or at the Castro Ridges. We conclude that the two different volcanic structures are fed from different melt batches from the melting region in the mantle and ascend through a similar lithospheric plumbing system.

6.3. Melt Ascent in the D. João de Castro Magmatic System

The compositional variability of the D. João de Castro lavas reflects the source and conditions of melting in the mantle but also yields important insights about ascent conditions in the crust. The combination of structural and geochemical observations allows determining how melts are transported from the mantle through the crust and along the rift system.

Lavas from D. João de Castro and the Castro Ridges range from alkali basalts to trachytes (Figure 5a). The mafic basalts and trachybasalts from D. João de Castro erupt without enhanced crystal fractionation in the crust, whereas the felsic lavas indicate periods of stagnation at different crustal levels and fractionation to trachyandesite and trachyte composition, respectively (Figure 5a). The distribution of lavas with varying degrees of fractionation is, however, not systematically restricted to a specific area or a certain distance relative to the main seamount, that is, mafic to evolved lavas occur on all volcanic structures (Figure 7). At the Castro Ridges, only a single sample has MgO contents <3 wt. %, indicating that extensive fractional crystallization influences lavas erupted at the central edifice. We note, however, that this could also be the result of denser sampling at the main edifice compared to the Castro Ridges. Contrastingly, the Santa

Bárbara magmatic system on the neighboring island Terceira displays a bimodal distribution between the Santa Bárbara central volcano, which erupts intermediate and evolved lavas and the fissure system that extends >10 km offshore to form the Serreta Ridge, which erupts mostly mafic lavas (Figure 7, Madureira et al., 2017). Both at D. João de Castro volcano and the Castro Ridges a large proportion of lavas are mafic, with the highest MgO contents occurring close to the volcano's center (Figure 7). This indicates that mafic melts may pass through the uppermost crust beneath the edifice and the volcanic rift zones and possibly accumulate olivine-clinopyroxene-rich crystal mush in a shallow magma reservoir beneath the central volcano before erupting (Cashman et al., 2017).

The Santa Bárbara volcano on Terceira is part of a mature magmatic system where ascending mafic melts stagnate in the plumbing system and are laterally transported along the mid-crustal rift zone to the offshore Serreta Ridge (Romer et al., 2019). Santa Bárbara central volcano also developed a large caldera with numerous felsic lava domes (Self, 1976), which is in contrast to the occurrence of both mafic and evolved lavas at D. João de Castro. The abundance of mafic lavas on the seamount suggests that the plumbing system beneath the edifice is less mature and ascending mafic melts can erupt without extensive crystallization compared to Santa Bárbara or Sete Cidades volcano on São Miguel (Beier et al., 2006; Romer et al., 2019). The abundance of olivine-clinopyroxene-rich lavas indicates interaction with crustal magma bodies where the crystals are mobilized. The presence of intermediate and evolved lavas at D. João de Castro, however, shows that fractional crystallization also is an important process during the ascent of melts and the evolution of the edifice. Thus, we suggest that the D. João de Castro seamount is an evolving central volcano on an active rift system with a high proportion of erupted mafic melt. As opposed to the more evolved, mature volcanoes on the islands, the seamount represents an early stage in the evolution of a central volcano.

6.4. Melt Transport and Volcano Growth in Active Rift Systems

In slowly diverging rift systems, large polygenetic volcanoes commonly form as a result of magma focusing within segments along the rift axis (Beutel et al., 2010; Sauter & Cannat, 2010). In order to understand how a central volcano such as D. João de Castro initially forms and develops further, it is crucial to understand the processes that influence the melt transport from the mantle through the crust. The formation of large central volcanoes requires the presence of a shallow magma chamber (Burchardt & Gudmundsson, 2009). These upper crustal magma reservoirs act as sinks for mafic melts that ascend via dikes from the deeper crust as well as serving as sources for fractionated melts that erupt from the central edifice (Gudmundsson, 2020). The deep situated reservoir of ocean islands is frequently located around the Moho from which mafic to intermediate melts are feeding fissure zones and replenishing the shallow magma reservoir (Klügel et al., 2015).

In young magmatic systems, for example, small seamounts, melts that are stored in the lithospheric mantle are transported subvertically to the surface without significant stagnation (Klügel et al., 2015). Mature magmatic systems associated with large central volcanoes form when the deep situated magma reservoir expands vertically and laterally leading to enhanced melt accumulation at the crust-mantle boundary as a result of dike arrest and deflection and subsequent trapping of further ascending dikes (Kühn & Dahm, 2008). Shallow crustal magma reservoirs are formed by repeated injection of dikes from large lower crustal and upper mantle reservoirs (Gudmundsson, 2011). Dike injection may result in arrest or deflection to sills in the upper crust, where low-density layers or elevated temperatures along with higher viscosities are an obstacle for the propagating mafic dikes (Menand, 2011). Based on geophysical studies, the depth for the crust-mantle boundary in the Azores ranges from 13 to 17 km (Spieker et al., 2018), and a recent study indicates a range from 10 to 16.5 km with shallower depths closer to the MAR (Ferreira et al., 2020). These observations are consistent with the prevalent depth of stagnation inferred from thermobarometric studies on selected volcanic islands (Romer et al., 2019; Zanon & Frezzotti, 2013; Zanon & Pimentel, 2015). Shallow magma chambers beneath other Azorean central volcanoes are located between 2 and 7 km (Beier et al., 2006; Dias et al., 2007; Jeffery et al., 2016, 2017; Romer et al., 2019). We suggest that D. João de Castro's shallow reservoir is located at a comparable depth interval beneath the central volcano and that the variable degree of fractionation indicates that melts derive from both a deep magma reservoir and from a shallow magma reservoir where extensive cooling and crystal fractionation occurs prior to eruption.

The formation of a shallow magma chamber is accompanied by changes in the lithospheric stress field. The circumferential orientation of volcanic structures at D. João de Castro (Figures 2 and 8b) shows that the regional tectonic stress field is superimposed by the local influence of a shallow magma chamber, where the overpressure results in radiating σ_1 stress trajectories (Burchardt et al., 2018; Gudmundsson & Brenner, 2004). In contrast, the Castro Fissure Zone, including the Castro Ridges, is formed from dike injections directly from the deep-seated reservoir in a northwesterly direction from D. João de Castro. The orientation of the entire fissure zone volcanism is controlled by the regional tectonic stress field in the NW Hirondelle Basin.

The presence of both mafic and evolved lavas from deep and shallow magma reservoirs implies that D. João de Castro has not reached a mature stage of evolution like those of the neighboring subaerial volcanoes (e.g., Santa Bárbara or Sete Cidades). The Castro Ridges are of predominantly mafic rock composition, however as opposed to the volcanic structures further to the NW, they are more massive and cannot easily be distinguished into single monogenetic cones. Based on the bathymetry and seismic imagery, however, the Castro Ridges are formed by clusters of individual cones that are concentrated along this section of the rift axis (Figures 3 and 4b). These structures and the occurrence of few basaltic-trachyandesites and trachyandesites indicates that continuous dike injections have led to deflection and initial sill formation in the upper crust (Figure 8a). Therefore, we conclude that volcanic ridges such as the Castro Ridges represent the initial phase in the formation of a central volcano in rift systems.

Based on the structural analysis of the fault scarps and volcano orientations, this initial phase is dominated by the regional tectonic stress field (Figures 2 and 8a), resulting in NW-SE striking elongated morphological patterns. Once a shallow magma chamber is established, the regional stress field-controlled morphology is overprinted by the subcircular morphology of the evolving central volcano (Figure 8b). D. João de Castro represents this transitional phase of evolution from a predominantly mafic volcanic system toward a polygenetic central volcano. A comparably weak upper crustal stress barrier leads to the occurrence of both mafic and highly fractionated lavas that occur radially around the volcano's center. In addition, mafic dikes that get hampered at upper crustal levels, for example, at the base of the volcanic edifice, either stall or are deflected and propagate laterally along the rift zone, bypassing the stress barrier and erupting at the Castro Fissure Zone (Figure 8b; Gudmundsson, 2020).

Continued injections of mafic dikes into the upper crust may then facilitate the growth of the shallow magma chamber, and the proportion of dikes that erupt directly from the deep reservoir decreases whereas the portion of dikes propagating into the fissure zone increases (Klügel et al., 2015). This process leads to the formation of a mature magmatic system with a bimodal distribution in the degree of fractionation between the central volcano and the fissure zone, comparable to the Santa Bárbara magmatic system (Figure 8c). The continuing growth of the shallow magma chamber may ultimately lead to the formation of a collapse caldera and the injection of cone sheets (Galland et al., 2014).

6.5. Geometry of Magmatic Segments Along the Terceira Rift

The positioning of D. João de Castro in the Terceira Rift as a relatively young central volcano allows determining the magma flow along the Terceira Rift. The Terceira Rift comprises features of both oceanic spreading ridges and continental rift systems (Beier et al., 2008). The Terceira Rift is located on a thick lithosphere between ~35 km close to the MAR and ~75 km in the southeast at São Miguel (Spieker et al., 2018), which results in deep generation of alkaline melts comparable to continental rifts (Figure 5, Beier et al., 2012). Similar to both oceanic and continental diverging systems, the Terceira Rift displays a regular pattern of amagmatic areas (basins) and magmatic centers like volcanic islands, volcanic ridges and seamounts, for example, at the Gakkel Ridges (Michael et al., 2003) or the East African Rift system (Ebinger et al., 2013). At diverging systems, the segmentation pattern is inferred to be generated by focused mantle melts from the asthenosphere producing locally thinned lithosphere and a thickened crust (Carbotte et al., 2015). The regularity in the spacing of the magmatic systems is associated with the diapiric ascent of Rayleigh-Taylor type gravitational instabilities in the partially molten mantle which leads to local upwelling zones of the asthenosphere and focused melt supply systems (Schouten et al., 1985).

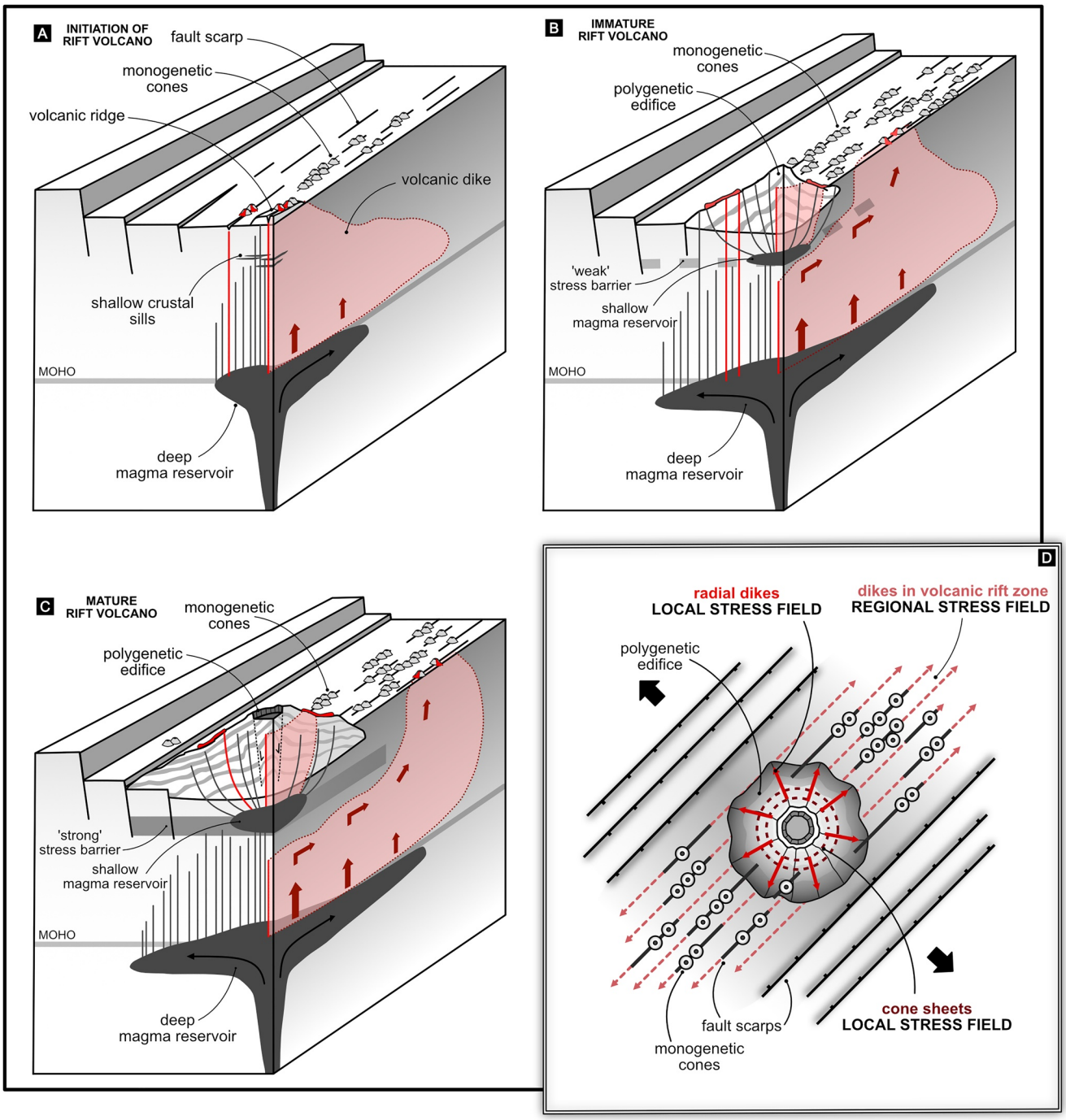

Figure 8. Schematic three-dimensional lithospheric profile through a (slow-diverging) rift system, showing the initiation and the evolution of a central volcano and the melt transport characteristics in the lower and upper crust. Melts are transported from a deep-seated magma reservoir located around the Moho via near vertical dikes toward the surface, where (a) they erupt, forming monogenetic cones and in part deflect into sills. The formation of sills results in the formation of elongated volcanic ridges, as a result of accumulation of monogenetic cones along areas with high volcanic activity. (b) Sills develop into a shallow magma chamber that acts as pool for ascending melts from the deep reservoir and source for more fractionated melts that form the edifice. The shallow magma reservoir influences the stress patterns in the upper crust and superimposes the regional tectonic stress field prevailing in the rift system resulting in the formation of a subcircular edifice with radiating volcanic structures. (c) The growth of the shallow magma chamber and changed crustal stress conditions leads to further trapping of ascending mafic melts and also forces dikes to propagate along the rift system bypassing the edifice. (d) Simplified bird's-eye view of the volcanic stage shown in (c) with highlighted potential melt pathways based on regional and local stress fields. Based on models and modified from Gudmundsson (2016) and Klügel et al. (2015). Not to scale.

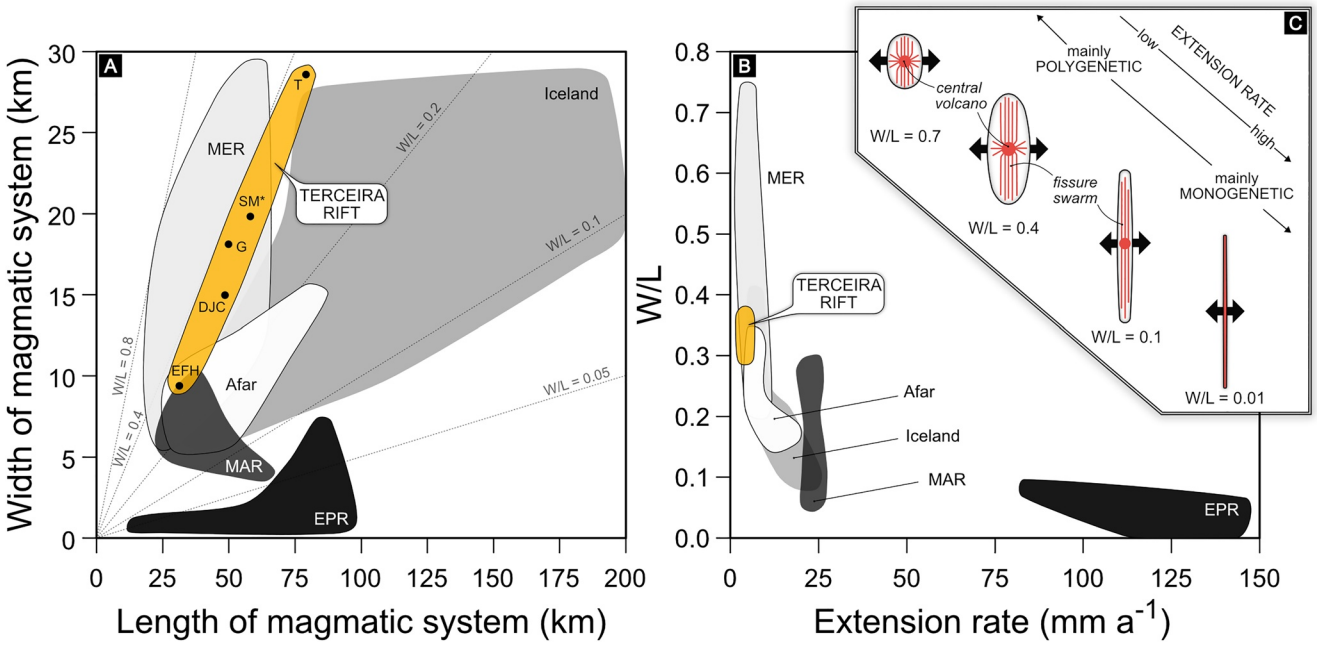

Figure 9. Relationship between (a) the width (*W*) and length (*L*) and (b) W/L ratio and extension rate of magmatic systems along the Terceira Rift in comparison with other oceanic and continental rift systems from the literature. Data sources in (a) and (b) are from Acocella (2014) and from Smith et al. (1995) for geometry data and DeMets et al. (2010) extension rates of the Mid-Atlantic Ridge (MAR), respectively. (c) Model showing the relationship between extension rate and the geometry of a magmatic segment in rift systems. Modified from Acocella (2014).

Along the Terceira Rift, the volcanic islands and D. João de Castro seamount are the surface expression of the magmatic segment where melts are focused (Beier et al., 2008; Vogt & Jung, 2004). The magmatic centers along the Terceira Rift have a regular spacing of ~80–100 km (Lourenço et al., 1998; Marques et al., 2013), whereas offsets, for example, in the Hirondelle Basin (Figure 1b) show that the magmatic segments are shifted against each other. In slowly diverging rift systems like in the Main Ethiopian Rift (MER), the deformation at segment centers is mainly magmatically induced, whereas the edges are tectonically, brittlely deformed (Corti, 2009). Similarly, basins between the volcanic islands and seamounts along the Terceira Rift represent the edges of the segments, where volcanism appears to be absent or sparse, and extension occurs by normal faulting (e.g., at Central Hirondelle Horst, Figure 4c).

The geometry of magmatic segments in rift system is controlled by the rate of extension. Acocella (2014) showed that the ratio between the width (W) and the length (*L*) of magmatic segments in rift systems increases as the extension rate decreases (Figure 9). At an extension rate of <25 mm/a the length of Icelandic magmatic systems (up to 200 km) is much greater compared to the East Pacific Rise, however, resulting in a W/L ratio of 0.1–0.3 considering the large widths between ~10 and 25 km. The East Pacific Rise has extremely high extension rates between 75 and 150 mm/a. The segment lengths are between 25 and 100 km but are also extremely narrow with widths that are commonly around ~1 km resulting in W/L ratios of <0.05. In contrast, continental rift system, such as Afar and the MER, have high *W*/*L* ratios between 0.2 and 0.8, reflecting their generally lower extension rates of <18 mm/a.

The lengths and widths of magmatic segments along the Terceira Rift are variable between the volcanic islands, for example, the western part of São Miguel is ~60 km long and ~20 km wide compared to the 30 km long and 10 km wide East Formigas High. The W/L ratios of all volcanic systems are, however, remarkably similar between 0.3 and 0.4 (Figure 9, Table 1) at very low extension rates of ~4 mm/a (Vogt & Jung, 2004). The comparably high W/L ratios of the segments along the Terceira Rift and the low overall extension rate shows that this rift system is very similar to the MER and Afar continental rift systems (Figure 9). Additionally, magmatic centers along the Terceira Rift exclusively erupt alkaline melts (Figure 5a) from low degree melting beneath thick lithosphere (Beier, Haase, et al., 2018) and have large crustal thicknesses (Gente et al., 2003) atypical for slow-spreading oceanic ridges (Cannat, 1996). There is no clear evidence for

Table 1
Overview of the Mean Widths (W) and Lengths (L) of Magmatic Segments Along the Terceira Rift (This Study) and the Mid-Atlantic Ridge (MAR) (Smith et al., 1995) and Resulting W/L Ratios. For the Determination of Single W and L Values of the Magmatic Systems Along the Terceira Rift a Regular 5 × 5 km Grid was Added to the Bathymetric Map. The Widths and Lengths Were Measured From the Map Every 5 km and Then Averaged. The Standard Deviation (SD) and Number of Values (n) Contributing to the Mean Value for Each Segment are Indicated. The Extension Rates for the Terceira Rift and the MAR are From Vogt and Jung (2004) and DeMets et al. (2010), Respectively

Magmatic segment	*W* (km)	SD	*n*	*L* (km)	SD	*n*	*W*/*L*	Extension rate (mm × a^{-1})
Graciosa	18.1	7.4	12	50.1	10.8	7	0.36	4.4
Terceira	31.9	4.6	15	79.1	8.1	13	0.40	4.4–4.2
D. João de Castro	15.0	6.3	10	48.5	2.1	4	0.31	4.2–4.0
São Miguel*	19.8	7	13	58.1	5.4	5	0.34	4.0–3.9
East Formigas High	9.4	2.7	7	31.3	5.7	4	0.30	3.9–3.7
MAR 2	8	-	-	33	-	-	0.24	23.85 ± 1.1
MAR 3	7	-	-	48	-	-	0.15	22.9 ± 0.7
MAR 4	8	-	-	28	-	-	0.29	23.8 ± 2.0
MAR 5	10	-	-	38	-	-	0.26	20.76 ± 1.0
MAR 6	5	-	-	38	-	-	0.13	23.8 ± 0.6
MAR 7	5	-	-	29	-	-	0.17	23.6 ± 0.6
MAR 8	6	-	-	33	-	-	0.18	23.45 ± 1.3
MAR 9	6	-	-	24	-	-	0.25	22.6
MAR 10	5	-	-	57	-	-	0.09	24.38 ± 0.9
MAR 11	5	-	-	57	-	-	0.09	24.07 ± 1.15
MAR 12	5	-	-	44	-	-	0.11	24.95 ± 0.89
MAR 13	4	-	-	64	-	-	0.06	22.1 ± 0.99

*The geometry of the São Miguel magmatic systems, solely derive from the westernmost Sete Cidades volcano and associated volcanic rift zone because the more eastern volcanoes are not dominated by the regional SW-NE extension along the Terceira Rift, but situated on a transform fault (Sibrant et al., 2016). MAR: Mid-Atlantic Ridge.

ocean seafloor spreading at the Terceira, neither geochemically (Storch et al., 2020) nor from gravity data (Luis et al., 1998) or geophysical data excluding extensive lithosphere thinning (Spieker et al., 2018). This along with the geometric similarities of magmatic segments along the Terceira Rift and the MER (Figure 9) suggests that initial oceanic rifts may be comparable to slow-diverging continental rifts rather than oceanic spreading centers.

The magmatic systems along the Terceira Rift are located on a lithosphere that varies in thickness of ~40 km from Graciosa to São Miguel (Beier et al., 2013). The increasing lithosphere thickness with increasing distance from the MAR, however, does not affect the geometry of the magmatic systems, showing that it is controlled by shallower crustal processes rather than the far-field stress field. As opposed to the Terceira Rift, the crustal thickness at the MER and Afar rift is very variable (18–40 km) and correlated with variable extension rates (Acocella, 2014). The low extension rates along the Terceira Rift (~4 mm/a) and comparably homogeneous crustal thicknesses (10–17 km) (Ferreira et al., 2020; Spieker et al., 2018) result in the formation of magmatic segments with consistent geometry, that is comparable to continental rift systems. Thus, we conclude that the extension rate and crustal thickness are controlling the geometry of magmatic systems.

7. Conclusions

The D. João de Castro seamount in the NW Hirondelle Basin is a solitaire central volcano defining a magmatic segment along the ultraslow diverging Terceira Rift in the Azores. Northwest of the edifice the N and NW Castro Ridges form part of a volcanic fissure zone (Castro Fissure Zone). The orientation of fault

scarps and volcanic structures at D. João de Castro and the fissure zone display that the morphology in the NW Hirondelle Basin is predominantly controlled by the regional SW-NE extending stress field. The regional tectonic stress field controls the melt pathways in the crust and leads to dike emplacement along the fissure zone and eruption of predominantly mafic lavas. The presence of mafic along with intermediate and evolved lavas at D. João de Castro indicates the presence of a shallow magma chamber beneath the seamount, which generates a subordinate local stress field and circumferential volcanic structures at the edifice.

Strontium-Nd-Pb isotope data along with incompatible trace element ratios show that D. João de Castro and the Castro Ridges originated from a small-scale heterogeneous mantle source. We propose a model in which D. João de Castro volcano formed from the growth of volcanic ridges, and by the formation of a shallow magma chamber that forced dike systems to deflect into sills. This leads to shallow stagnation of melts that ascend from a deep-seated reservoir accompanied by dike deflection at upper crustal stress barriers (e.g., the base of the volcanic edifice) and propagation and eruption along the fissure zone. The geometry of D. João de Castro and other magmatic systems along the Terceira Rift and the alkalic nature of the lavas, as well as the large lithosphere thickness, indicates that the Terceira Rift is more similar to continental rift systems than to oceanic spreading centers

D. João de Castro is one of the few examples globally in which the transition from ridge volcanism to the establishment of a large, central intraplate volcano can be observed. This model may be applicable to the volcanic systems along the Terceira Rift and other volcanically active rift systems that may initiate in areas in which the structural integrity of the crust controls much of the early stages of volcanism. Continuous diking and magma stagnation in the crust and the associated cooling and fractionation will then lead to the establishment of a central volcano.

Data Availability Statement

The data is available in the PANGAEA data repository at https://doi.org/10.1594/PANGAEA.932080.

Acknowledgments
The authors acknowledge help and support from captains M. Schneider and J.F. Schubert, crews and scientists during M113 and M128 for their friendly support. A special thanks to M. Regelous for support in the Erlangen clean laboratories. They acknowledge the constructive and helpful reviews by two anonymous reviewers and editorial handling by L. Jolivet. R. Romer and C. Hübscher thank B. Könich Schleifer, Prinz W. H., F. K. Kemner, B. F. Storch, F. B. Genske, and S.H. Krumm for their invaluable support during the sampling. C. Hübscher acknowledges P. Hills for support. All new geochemical data used in this study can be found in supplemental Tables S1 and S2 along with lithological information on D. João de Castro in Figure S1. This study was funded by the Deutsche Forschungsgemeinschaft (DFG grant BE4459/9-1). Open access funding enabled and organized by Projekt DEAL.

References

Acocella, V. (2014). Structural control on magmatism along divergent and convergent plate boundaries: Overview, model, problems. *Earth-Science Reviews*, *136*, 226–288. https://doi.org/10.1016/j.earscirev.2014.05.006

Acocella, V., & Neri, M. (2009). Dike propagation in volcanic edifices: Overview and possible developments. *Tectonophysics*, *471*, 67–77. https://doi.org/10.1016/j.tecto.2008.10.002

Agranier, A., Blichert-Tofta, J., Graham, D., Debaille, V., Schiano, P., Albarède, F., et al. (2005). The spectra of isotopic heterogeneities along the mid-Atlantic Ridge. *Earth and Planetary Science Letters*, *238*, 96–109. https://doi.org/10.1016/j.epsl.2005.07.011

Asimow, P. D., Dixon, J. E., & Langmuir, C. H. (2004). A hydrous melting and fractionation model for mid-ocean ridge basalts: Application to the Mid-Atlantic Ridge near the Azores. *Geochemistry, Geophysics, Geosystems*, *5*. https://doi.org/10.1029/2003gc000568

Béguelin, P., Bizimis, M., Beier, C., & Turner, S. (2017). Rift–plume interaction reveals multiple generations of recycled oceanic crust in Azores lavas. *Geochimica et Cosmochimica Acta*, *218*, 132–152. https://doi.org/10.1016/j.gca.2017.09.015

Beier, C., Bach, W., Blum, M., Cerqueira, T., Ferreira, P. J., Genske, F. S., et al. (2017). *Azores Plateau - Cruise No. M128 - July 02, 2016 - July 27, 2016 - Ponta Delgada (Portugal) - Ponta Delgada (Portugal) -METEOR-Berichte* (p. 41). DFG-Senatskommission für Ozeanographie. https://doi.org/10.2312/cr_m128

Beier, C., Brandl, P. A., Lima, S. M., & Haase, K. M. (2018). Tectonic control on the genesis of magmas in the New Hebrides arc (Vanuatu). *Lithos*, *312*, 290–307. https://doi.org/10.1016/j.lithos.2018.05.011

Beier, C., Haase, K. M., Abouchami, W., Krienitz, M. S., & Hauff, F. (2008). Magma genesis by rifting of oceanic lithosphere above anomalous mantle: Terceira Rift, Azores. *Geochemistry, Geophysics, Geosystems*, *9*, 27–55. https://doi.org/10.1029/2008gc002112

Beier, C., Haase, K. M., & Brandl, P. A. (2018). Melting and mantle sources in the Azores. In U. Kueppers, & C. Beier (Eds.), *Volcanoes of the Azores: Revealing the geological secrets of the central northern Atlantic islands* (pp. 251–280). Heidelberg: Springer Berlin. https://doi.org/10.1007/978-3-642-32226-6_11

Beier, C., Haase, K. M., & Hansteen, T. H. (2006). Magma evolution of the Sete Cidades volcano, São Miguel, Azores. *Journal of Petrology*, *47*(7), 1375–1411. https://doi.org/10.1093/petrology/egl014

Beier, C., Haase, K. M., & Turner, S. P. (2012). Conditions of melting beneath the Azores. *Lithos*, *144*, 1–11. https://doi.org/10.1016/j.lithos.2012.02.019

Beier, C., Mata, J., Stöckhert, F., Mattielli, N., Brandl, P. A., Madureira, P., et al. (2013). Geochemical evidence for melting of carbonated peridotite on Santa Maria Island, Azores. *Contributions to Mineralogy and Petrology*, *165*(5), 823–841. https://doi.org/10.1007/s00410-012-0837-2

Beier, C., Stracke, A., & Haase, K. M. (2007). The peculiar geochemical signatures of São Miguel (Azores) lavas: Metasomatised or recycled mantle sources? *Earth and Planetary Science Letters*, *259*, 186–199. https://doi.org/10.1016/j.epsl.2007.04.038

Beutel, E., van Wijk, J., Ebinger, C., Keir, D., & Agostini, A. (2010). Formation and stability of magmatic segments in the Main Ethiopian and Afar rifts. *Earth and Planetary Science Letters*, *293*, 225–235. https://doi.org/10.1016/j.epsl.2010.02.006

Bonatti, E. (1990). Not so hot "hot spots" in the oceanic mantle. *Science*, *250*, 107–111.

Bourdon, B., Turner, S. P., & Ribe, N. M. (2005). Partial melting and upwelling rates beneath the Azores from a U-series isotope perspective. *Earth and Planetary Science Letters*, *239*, 42–56. https://doi.org/10.1016/j.epsl.2005.08.008

Brandl, P. A., Beier, C., Regelous, M., Abouchami, W., Haase, K. M., Garbe-Schönberg, D., & Galer, S. J. G. (2012). Volcanism on the flanks of the East Pacific Rise: Quantitative constraints on mantle heterogeneity and melting processes. *Chemical Geology*, *298*, 41–56. https://doi.org/10.1016/j.chemgeo.2011.12.015

Burchardt, S., & Gudmundsson, A. (2009). The infrastructure of Geitafell volcano, southeast IcelandIAVCEIStudies in Volcanology: The Legacy of George Walker. Spec. Publ. of (Vol. 2, pp. 349–370).

Burchardt, S., Walter, T. R., & Tuffen, H. (2018). Growth of a volcanic edifice through plumbing system processes: Volcanic rift zones. *Magmatic sheet-intrusion swarms and long-lived conduits, volcanic and igneous plumbing systems* (pp. 89–112). Elsevier. https://doi.org/10.1016/b978-0-12-809749-6.00004-2

Cande, S. C., & Kent, D. V. (1995). Revised calibration of the geomagnetic polarity timescale for the Late Cretaceous and Cenozoic. *Journal of Geophysical Research*, *100*, 6093–6095. https://doi.org/10.1029/94jb03098

Cannat, M. (1996). How thick is the magmatic crust at slow spreading oceanic ridges? *Journal of Geophysical Research*, *101*, 2847–2857. https://doi.org/10.1029/95jb03116

Cannat, M., Briais, A., Deplus, C., Escartin, J., Georgen, J., Lin, J., et al. (1999). Mid-Atlantic Ridge–Azores hotspot interactions: Along-axis migration of a hotspot-derived event of enhanced magmatism 10 to 4 Ma ago. *Earth and Planetary Science Letters*, *173*, 257–269. https://doi.org/10.1016/s0012-821x(99)00234-4

Cannat, M., Mevel, C., Maia, M., Deplus, C., Durand, C., Gente, P., et al. (1995). Thin crust, ultramafic exposures, and rugged faulting patterns at the Mid-Atlantic Ridge (22–24 N). *Geology*, *23*, 49–52. https://doi.org/10.1130/0091-7613(1995)023<0049:tcuear>2.3.co;2

Carbotte, S. M., & Macdonald, K. C. (1994). The axial topographic high at intermediate and fast spreading ridges. *Earth and Planetary Science Letters*, *128*, 85–97. https://doi.org/10.1016/0012-821x(94)90137-6

Carbotte, S. M., Smith, D. K., Cannat, M., & Klein, E. M. (2015). Tectonic and magmatic segmentation of the Global Ocean Ridge system: A synthesis of observations. *Geological Society, London, Special Publications*, *420*, 249–295. https://doi.org/10.1144/sp420.5

Cardigos, F., Colaço, A., Dando, P.R., Ávila, S. P., Sarradin, P.-M., Tempera, F., Conceição, P., et al. (2005). Shallow water hydrothermal vent field fluids and communities of the D. João de Castro Seamount (Azores). *Chemical Geology*, *224*, 153–168. https://doi.org/10.1016/j.chemgeo.2005.07.019

Carmo, R., Madeira, J., Ferreira, T., Queiroz, G., & Hipólito, A. (2015). Volcano-tectonic structures of São Miguel Island, Azores. *Geological Society, London, Memoirs*, *44*(1), 65–86. https://doi.org/10.1144/m44.6

Casalbore, D., Romagnoli, C., Pimentel, A., Quartau, R., Casas, D., Ercilla, G., et al. (2015). Volcanic, tectonic and mass-wasting processes offshore Terceira Island (Azores) revealed by high-resolution seafloor mapping. *Bulletin of Volcanology*, *77*, 24. https://doi.org/10.1007/s00445-015-0905-3

Casas, D., Pimentel, A., Pacheco, J., Martorelli, E., Sposato, A., Ercilla, G., et al. (2018). Serreta 1998–2001 submarine volcanic eruption, offshore Terceira (Azores): Characterization of the vent and inferences about the eruptive dynamics. *Journal of Volcanology and Geothermal Research*, *356*, 127–140. https://doi.org/10.1016/j.jvolgeores.2018.02.017

Cashman, K. V., Sparks, R. S. J., & Blundy, J. D. (2017). Vertically extensive and unstable magmatic systems: A unified view of igneous processes. *Science*, *355*. https://doi.org/10.1126/science.aag3055

Chiocci, F. L., Romagnoli, C., Casalbore, D., Sposato, A., Martorelli, E., Alonso, B., et al. (2013). Bathy-morphological setting of Terceira Island (Azores) after the FAIVI cruise. *Journal of Maps*, *9*(4), 590–595. https://doi.org/10.1080/17445647.2013.831381

Compston, W., & Oversby, V. M. (1969). Lead isotopic analysis using a double spike. *Journal of Geophysical Research*, *74*, 4338–4348. https://doi.org/10.1029/jb074i017p04338

Corti, G. (2009). Continental rift evolution: From rift initiation to incipient break-up in the Main Ethiopian Rift, East Africa. *Earth-Science Reviews*, *96*, 1–53. https://doi.org/10.1016/j.earscirev.2009.06.005

Delcamp, A., Poppe, S., Detienne, M., & Paguican, E. (2018). *Destroying a volcanic edifice: Interactions between edifice instabilities and the volcanic plumbing system, volcanic and igneous plumbing systems* (pp. 231–257). Elsevier. https://doi.org/10.1016/b978-0-12-809749-6.00009-1

DeMets, C., Gordon, R. G., & Argus, D. F. (2010). Geologically current plate motions. *Geophysical Journal International*, *181*, 1–80. https://doi.org/10.1111/j.1365-246x.2009.04491.x

Dias, N. A., Matias, L., Lourenço, N., Madeira, J., Carrilho, F., Gaspar, J. L. (2007). Crustal seismic velocity structure near Faial and Pico Islands (AZORES), from local earthquake tomography. *Tectonophysics*, *445*, 301–317. https://doi.org/10.1016/j.tecto.2007.09.001

Dick, H. J., Lin, J., & Schouten, H. (2003). An ultraslow-spreading class of ocean ridge. *Nature*, *426*(6965), 405–412. https://doi.org/10.1038/nature02128

Dosso, L., Bougault, H., Langmuir, C., Bollinger, C., Bonnier, O., & Etoubleau, J. (1999). The age and distribution of mantle heterogeneity along the Mid-Atlantic Ridge (31–41 N). *Earth and Planetary Science Letters*, *170*, 269–286. https://doi.org/10.1016/s0012-821x(99)00109-0

Ebinger, C. J., Jackson, J., Foster, A., & Hayward, N. (1999). Extensional basin geometry and the elastic lithosphere. *Philosophical Transactions of the Royal Society of London Series A: Mathematical, Physical and Engineering Sciences*, *357*, 741–765. https://doi.org/10.1098/rsta.1999.0351

Ebinger, C. J., van Wijk, J., & Keir, D. (2013). The time scales of continental rifting: Implications for global processes. *Geological Society of America Special Paper*, *500*, 371–396. https://doi.org/10.1130/2013.2500(11)

Elliott, T., Blichert-Toft, J., Heumann, A., Koetsier, G., & Forjaz, V. (2007). The origin of enriched mantle beneath Sao Miguel, Azores. *Geochimica et Cosmochimica Acta*, *71*, 219–240. https://doi.org/10.1016/j.gca.2006.07.043

Ferreira, A. M., Marignier, A., Attanayake, J., Frietsch, M., & Berbellini, A. (2020). Crustal structure of the Azores Archipelago from Rayleigh wave ellipticity data. *Geophysical Journal International*, *221*, 1232–1247. https://doi.org/10.1093/gji/ggaa076

Freund, S., Beier, C., Krumm, S., & Haase, K. M. (2013). Oxygen isotope evidence for the formation of andesitic–dacitic magmas from the fast-spreading Pacific–Antarctic Rise by assimilation–fractional crystallisation. *Chemical Geology*, *347*, 271–283. https://doi.org/10.1016/j.chemgeo.2013.04.013

Gale, A., Escrig, S., Gier, E. J., Langmuir, C. H., & Goldstein, S. L. (2011). Enriched basalts at segment centers: The Lucky Strike (37 17′ N) and Menez Gwen (37 50′ N) segments of the Mid-Atlantic Ridge. *Geochemistry, Geophysics, Geosystems*, *12*. https://doi.org/10.1029/2010gc003446

Gale, A., Laubier, M., Escrig, S., & Langmuir, C. H. (2013). Constraints on melting processes and plume-ridge interaction from comprehensive study of the FAMOUS and North Famous segments, Mid-Atlantic Ridge. *Earth and Planetary Science Letters*, *365*, 209–220. https://doi.org/10.1016/j.epsl.2013.01.022

Galland, O., Burchardt, S., Hallot, E., Mourgues, R., & Bulois, C. (2014). Dynamics of dikes versus cone sheets in volcanic systems. *Journal of Geophysical Research: Solid Earth*, *119*, 6178–6192. https://doi.org/10.1002/2014jb011059

Geist, D. J., Fornari, D. J., Kurz, M. D., Harpp, K. S., Soule, S. A., Perfit, M. R., Koleszar, A. M. (2006). Submarine Fernandina: Magmatism at the leading edge of the Galápagos hot spot. *Geochemistry, Geophysics, Geosystems*, *7*. https://doi.org/10.1029/2006gc001290

Gente, P., Dyment, J., Maia, M., & Goslin, J. (2003). Interaction between the Mid-Atlantic Ridge and the Azores hot spot during the last 85 Myr: Emplacement and rifting of the hot spot-derived plateaus. *Geochemistry, Geophysics, Geosystems*, *4*. https://doi.org/10.1029/2003gc000527

Gudmundsson, A. (1987). Tectonics of the Thingvellir fissure swarm, SW Iceland. *Journal of Structural Geology*, *9*, 61–69. https://doi.org/10.1016/0191-8141(87)90044-7

Gudmundsson, A. (1998). Magma chambers modeled as cavities explain the formation of rift zone central volcanoes and their eruption and intrusion statistics. *Journal of Geophysical Research*, *103*, 7401–7412. https://doi.org/10.1029/97jb03747

Gudmundsson, A. (2011). Deflection of dykes into sills at discontinuities and magma-chamber formation. *Tectonophysics*, *500*, 50–64. https://doi.org/10.1016/j.tecto.2009.10.015

Gudmundsson, A. (2016). The mechanics of large volcanic eruptions. *Earth-Science Reviews*, *163*, 72–93. https://doi.org/10.1016/j.earscirev.2016.10.003

Gudmundsson, A. (2020). *Volcanotectonics: Understanding the structure, deformation and dynamics of volcanoes* (p. 598). Cambridge University Press.

Gudmundsson, A., & Brenner, S. L. (2004). Local stresses, dyke arrest and surface deformation in volcanic edifices and rift zones. *Annals of Geophysics*, *47*, 1433–1454.

Haase, K. M., & Beier, C. (2003). Tectonic control of ocean island basalt sources on São Miguel, Azores? *Geophysical Research Letters*, *30*(16). https://doi.org/10.1029/2003gl017500

Haase, K. M., Beier, C., Regelous, M., Rapprich, V., & Renno, A. (2017). Spatial variability of source composition and petrogenesis in rift and rift flank alkaline lavas from the Eger Rift, Central Europe. *Chemical Geology*, *455*, 304–314. https://doi.org/10.1016/j.chemgeo.2016.11.003

Hamelin, C., Bezos, A., Dosso, L., Escartin, J., Cannat, M., & Mevel, C. (2013). Atypically depleted upper mantle component revealed by Hf isotopes at Lucky Strike segment. *Chemical Geology*, *341*, 128–139. https://doi.org/10.1016/j.chemgeo.2013.01.013

Hayward, N., & Ebinger, C. (1996). Variations in the along-axis segmentation of the Afar Rift system. *Tectonics*, *15*, 244–257. https://doi.org/10.1029/95tc02292

Heezen, B. C. (1960). The rift in the ocean floor. *Scientific American*, *203*, 98–110. https://doi.org/10.1038/scientificamerican1060-98

Hildenbrand, A., Weis, D., Madureira, P., & Marques, F. O. (2014). Recent plate re-organization at the Azores Triple Junction: Evidence from combined geochemical and geochronological data on Faial, S. Jorge and Terceira volcanic islands. *Lithos*, *210*, 27–39. https://doi.org/10.1016/j.lithos.2014.09.009

Hübscher, C., Christoph, B., Muayyad, A. H., Luis, B., Marie, B., Martina, B., et al. (2016). *Azores Plateau - Cruise No. M113/1 - December 29, 2014 - January 22, 2015 - Ponta Delgada (Portugal) - Ponta Delgada (Portugal)* (p. 31). METEOR-Berichte. DFG-Senatskommission für Ozeanographie. https://doi.org/10.2312/cr_m113_1

Hübscher, C., & Gohl, K. (2014). Reflection/refraction seismology. *Encyclopedia of marine geosciences* (pp. 1–15). New York: Springer.

Irvine, T. N., & Baragar, W. (1971). A guide to the chemical classification of the common volcanic rocks. *Canadian Journal of Earth Sciences*, *8*, 523–548. https://doi.org/10.1139/e71-055

Jeffery, A. J., Gertisser, R., O'Driscoll, B., Pacheco, J. M., Whitley, S., Pimentel, A., & Self, S. (2016). Temporal evolution of a post-caldera, mildly peralkaline magmatic system: Furnas volcano, São Miguel, Azores. *Contributions to Mineralogy and Petrology*, *171*, 42. https://doi.org/10.1007/s00410-016-1235-y

Jeffery, A. J., Gertisser, R., Self, S., Pimentel, A., O'Driscoll, B., & Pacheco, J. M. (2017). Petrogenesis of the peralkaline ignimbrites of Terceira, Azores. *Journal of Petrology*, *58*, 2365–2402. https://doi.org/10.1093/petrology/egy012

Karátson, D., Thouret, J.-C., Moriya, I., & Lomoschitz, A. (1999). Erosion calderas: Origins, processes, structural and climatic control. *Bulletin of Volcanology*, *61*, 174–193. https://doi.org/10.1007/s004450050270

Klügel, A., Longpré, M.-A., García-Cañada, L., & Stix, J. (2015). Deep intrusions, lateral magma transport and related uplift at ocean island volcanoes. *Earth and Planetary Science Letters*, *431*, 140–149. https://doi.org/10.1016/j.epsl.2015.09.031

Krause, D. C., & Watkins, N. D. (1970). North Atlantic Crustal Genesis in the vicinity of the Azores. *Geophysical Journal of the Royal Astronomical Society*, *19*, 261–283. https://doi.org/10.1111/j.1365-246x.1970.tb06046.x

Kühn, D., & Dahm, T. (2008). Numerical modelling of dyke interaction and its influence on oceanic crust formation. *Tectonophysics*, *447*, 53–65. https://doi.org/10.1016/j.tecto.2006.09.018

Kurz, T., Gloaguen, R., Ebinger, C., Casey, M., & Abebe, B. (2007). Deformation distribution and type in the Main Ethiopian Rift (MER): A remote sensing study. *Journal of African Earth Sciences*, *48*, 100–114. https://doi.org/10.1016/j.jafrearsci.2006.10.008

Larrea, P., Galé, C., Ubide, T., Widom, E., Lago, M., & França, Z. (2014). Magmatic Evolution of Graciosa (Azores, Portugal). *Journal of Petrology*, *55*, 2125–2154. https://doi.org/10.1093/petrology/egu052

LeMaitre, R. W. B., Dudek, P., Keller, A., Lameyre, J., Le Bas, J., Sabine, M. J., et al. (1989). *A classification of igneous rocks and glossary of terms: Recommendations of the International Union Of Geological Sciences, subcommission on the systematics of igneous rocks* (p. 193). International Union of Geological Sciences.

Lourenço, N., Miranda, J. M., Luis, J. F., Ribeiro, A., Victor, L. A. M., Madeira, J., & Needham, H. D. (1998). Morpho-tectonic analysis of the Azores Volcanic Plateau from a new bathymetric compilation of the area. *Marine Geophysical Researches*, *20*, 141–156. https://doi.org/10.1023/a:1004505401547

Luis, J. F., & Miranda, J. M. (2008). Reevaluation of magnetic chrons in the North Atlantic between 35 degrees N and 47 degrees N: Implications for the formation of the Azores Triple Junction and associated plateau. *Journal of Geophysical Research*, *113*. https://doi.org/10.1029/2007jb005573

Luis, J. F., Miranda, J. M., Galdeano, A., & Patriat, P. (1998). Constraints on the structure of the Azores spreading center from gravity data. *Marine Geophysical Researches*, *20*(3), 157–170. https://doi.org/10.1023/a:1004698526004

Madeira, J., Brum da Silveira, A., Hipólito, A., & Carmo, R. (2015). Active tectonics in the Central and Eastern Azores Islands along the Eurasia–Nubia boundary: A review. *Geological Society, London, Memoirs*, *44*, 15–32. https://doi.org/10.1144/m44.3

Madureira, P., Mata, J., Mattielli, N., Queiroz, G., & Silva, P. (2011). Mantle source heterogeneity, magma generation and magmatic evolution at Terceira Island (Azores archipelago): Constraints from elemental and isotopic (Sr, Nd, Hf, and Pb) data. *Lithos*, *126*, 402–418. https://doi.org/10.1016/j.lithos.2011.07.002

Madureira, P., Moreira, M., & Mata, J. (2005). The Azores hotspot: A lower mantle origin for Terceira magmas as shown by Ne isotopic data. *Geochimica et Cosmochimica Acta*, *69*, A106.

Madureira, P., Rosa, C., Marques, A. F., Silva, P., Moreira, M., Hamelin, C., et al. (2017). The 1998–2001 submarine lava balloon eruption at the Serreta ridge (Azores archipelago): Constraints from volcanic facies architecture, isotope geochemistry and magnetic data. *Journal of Volcanology and Geothermal Research*, *329*, 13–29. https://doi.org/10.1016/j.jvolgeores.2016.11.006

Marques, F. O., Catalão, J., Hildenbrand, A., & Madureira, P. (2015). Ground motion and tectonics in the Terceira Island: Tectonomagmatic interactions in an oceanic rift (Terceira Rift, Azores Triple Junction). *Tectonophysics*, *651*, 19–34. https://doi.org/10.1016/j.tecto.2015.02.026

Marques, F. O., Catalão, J. C., DeMets, C., Costa, A. C. G., & Hildenbrand, A. (2013). GPS and tectonic evidence for a diffuse plate boundary at the Azores Triple Junction. *Earth and Planetary Science Letters*, *381*, 177–187. https://doi.org/10.1016/j.epsl.2013.08.051

Menand, T. (2011). Physical controls and depth of emplacement of igneous bodies: A review. *Tectonophysics*, *500*, 11–19. https://doi.org/10.1016/j.tecto.2009.10.016

Mendel, V., Sauter, D., Rommevaux-Jestin, C., Patriat, P., Lefebvre, F., Parson, L. M., (2003). Magmato-tectonic cyclicity at the ultra-slow spreading Southwest Indian Ridge: Evidence from variations of axial volcanic ridge morphology and abyssal hills pattern. *Geochemistry, Geophysics, Geosystems*, *4*(5), 9102. https://doi.org/10.1029/2002gc000417

Métrich, N., Zanon, V., Créon, L., Hildenbrand, A., Moreira, M., & Marques, F. O. (2014). Is the 'Azores hotspot'a wetspot? Insights from the geochemistry of fluid and melt inclusions in olivine of Pico basalts. *Journal of Petrology*, *55*, 377–393. https://doi.org/10.1093/petrology/egt071

Michael, P., Langmuir, C. H., Dick, H. J. B., Snow, J. E., Goldstein, S. L., Graham, D. W., et al. (2003). Magmatic and amagmatic seafloor generation at the ultraslow-spreading Gakkel ridge, Arctic Ocean. *Nature*, *423*(6943), 956–961. https://doi.org/10.1038/nature01704

Miranda, J. M., Luis, J. F., & Lourenço, N. (2018). The tectonic evolution of the Azores Based on magnetic data. In U. Kueppers, & C. Beier (Eds.), *Volcanoes of the Azores: Revealing the geological secrets of the central northern Atlantic islands* (pp. 89–100). Heidelberg: Springer Berlin. https://doi.org/10.1007/978-3-642-32226-6_6

Mitchell, N. C., & Lofi, J. (2008). Submarine and subaerial erosion of volcanic landscapes: Comparing Pacific Ocean seamounts with Valencia Seamount, exposed during the Messinian salinity crisis. *Basin Research*, *20*, 489–502. https://doi.org/10.1111/j.1365-2117.2008.00355.x

Montelli, R., Nolet, G., Dahlen, F. A., Masters, G., Robert, E. E., Hung, S.-H. (2004). Finite-frequency tomography reveals a variety of plumes in the mantle. *Science*, *303*, 338–343. https://doi.org/10.1126/science.1092485

Moreira, M. A., Madureira, P., & Mata, J. (2018). Noble gas constraints on the origin of the Azores Hotspot. In U. Kueppers, & C. Beier (Eds.), *Volcanoes of the Azores: Revealing the geological secrets of the central northern Atlantic islands* (pp. 281–299). Berlin, Heidelberg: Springer. https://doi.org/10.1007/978-3-642-32226-6_12

Mutter, J. C., & Karson, J. A. (1992). Structural processes at slow-spreading ridges. *Science*, *257*, 627–634. https://doi.org/10.1126/science.257.5070.627

Nelson, C. H., Goldfinger, C., Johnson, J. E., & Dunhill, G. (2000). Variation of modern turbidite systems along the subduction zone margin of Cascadia Basin and implications for turbidite reservoir beds. *Deep-water reservoirs of the world: 20th annual research conference* (p. 31). Gulf Coast Section Society of Economic Paleontologists and Mineralogists.

Nemec, W. (1988). The shape of the rose. *Sedimentary Geology*, *59*, 149–152. https://doi.org/10.1016/0037-0738(88)90105-4

O'Neill, C., & Sigloch, K. (2018). Crust and mantle structure beneath the Azores hotspot: Evidence from geophysics. In U. Kueppers, & C. Beier (Eds.), *Volcanoes of the Azores: Revealing the geological secrets of the central northern Atlantic islands* (pp. 71–87). Berlin, Heidelberg: Springer.

Perfit, M. R., & Chadwick, W. W. (1998). Magmatism at mid-ocean ridges: Constraints from volcanological and geochemical investigations. Geophysical Monograph-American Geophysical Union (pp. 59–116). https://doi.org/10.1029/GM106p0059

Pimentel, A., Zanon, V., de Groot, L. V., Hipólito, A., Di Chiara, A., & Self, S. (2016). Stress-induced comenditic trachyte effusion triggered by trachybasalt intrusion: Multidisciplinary study of the AD 1761 eruption at Terceira Island (Azores). *Bulletin of Volcanology*, *78*, 22. https://doi.org/10.1007/s00445-016-1015-6

Pope, E. L., Jutzeler, M., Cartigny, M. J. B., Shreeve, J., Talling, P. J., Wright, I. C., & Wysoczanski, R. J. (2018). Origin of spectacular fields of submarine sediment waves around volcanic islands. *Earth and Planetary Science Letters*, *493*, 12–24. https://doi.org/10.1016/j.epsl.2018.04.020

Prytulak, J., & Elliott, T. (2007). TiO_2 enrichment in ocean island basalts. *Earth and Planetary Science Letters*, *263*, 388–403. https://doi.org/10.1016/j.epsl.2007.09.015

Robinson, J. A. C., & Wood, B. J. (1998). The depth of the spinel to garnet transition at the peridotite solidus. *Earth and Planetary Science Letters*, *164*, 277–284. https://doi.org/10.1016/s0012-821x(98)00213-1

Romer, R. H. W., Beier, C., Haase, K., Klügel, A., & Hamelin, C. (2019). Progressive changes in magma transport at the active Serreta Ridge, Azores. *Geochemistry, Geophysics, Geosystems*, *20*. https://doi.org/10.1029/2019GC008562

Romer, R. H. W., Beier, C., Haase, K. M., & Hübscher, C. (2018). Correlated changes between volcanic structures and magma composition in the Faial volcanic system, Azores. *Frontiers of Earth Science*, *6*, 78. https://doi.org/10.3389/feart.2018.00078

Rubin, K. H., & Sinton, J. M. (2007). Inferences on mid-ocean ridge thermal and magmatic structure from MORB compositions. *Earth and Planetary Science Letters*, *260*, 257–276. https://doi.org/10.1016/j.epsl.2007.05.035

Sauter, D., & Cannat, M. (2010). The ultraslow spreading Southwest Indian ridge. *J diversity of hydrothermal systems on slow-spreading ocean ridges* (pp. 153–173). https://doi.org/10.1029/2008gm000843

Schilling, J.-G. (1975). Azores mantle blob: Rare-earth evidence. *Earth and Planetary Science Letters*, *25*, 103–115. https://doi.org/10.1016/0012-821x(75)90186-7

Schilling, J.-G., Bergeron, M. B., Evans, R., & Smith, J. V. (1980). Halogens in the mantle beneath the North Atlantic [and discussion]. *Philosophical Transactions of the Royal Society of London A: Mathematical, Physical and Engineering Sciences*, *297*, 147–178. https://doi.org/10.1098/rsta.1980.0208

Schouten, H., Klitgord, K. D., & Whitehead, J. A. (1985). Segmentation of mid-ocean ridges. *Nature*, *317*, 225–229. https://doi.org/10.1038/317225a0

Schwarz, S., Klügel, A., & Wohlgemuth-Ueberwasser, C. (2004). Melt extraction pathways and stagnation depths beneath the Madeira and Desertas rift zones (NE Atlantic) inferred from barometric studies. *Contributions to Mineralogy and Petrology*, *147*, 228–240. https://doi.org/10.1007/s00410-004-0556-4

Self, S. (1976). The recent volcanology of Terceira, Azores. *Journal of the Geological Society*, *132*, 645–666. https://doi.org/10.1144/gsjgs.132.6.0645

Shen, Y., & Forsyth, D. W. (1995). Geochemical constraints on initial and final depths of melting beneath mid-ocean ridges. *Journal of Geophysical Research*, *100*, 2211–2237. https://doi.org/10.1029/94jb02768

Shirey, S. B., Bender, J. F., & Langmuir, C. H. (1987). Three-component isotopic heterogeneity near the Oceanographer transform, Mid-Atlantic Ridge. *Nature*, *325*, 217–223. https://doi.org/10.1038/325217a0

Sibrant, A. L. R., Marques, F. O., & Hildenbrand, A. (2014). Construction and destruction of a volcanic island developed inside an oceanic rift: Graciosa Island, Terceira Rift, Azores. *Journal of Volcanology and Geothermal Research*, *284*, 32–45. https://doi.org/10.1016/j.jvolgeores.2014.07.014

Sibrant, A. L. R., Marques, F. O., Hildenbrand, A., Boulesteix, T., Costa, A. C. G., & Catalão, J. (2016). Deformation in a hyperslow oceanic rift: Insights from the tectonics of the São Miguel Island (Terceira Rift, Azores). *Tectonics*, *35*, 425–446. https://doi.org/10.1002/2015tc003886

Sigurdsson, H., & Sparks, S. R. (1978). Lateral magma flow within rifted Icelandic crust. *Nature*, *274*, 126–130. https://doi.org/10.1038/274126a0

Smith, D. K., Humphris, S. E., & Bryan, W. B. (1995). A comparison of volcanic edifices at the Reykjanes Ridge and the Mid-Atlantic Ridge at 24°–30°N. *Journal of Geophysical Research*, *100*, 22485–22498. https://doi.org/10.1029/95jb02392

Spieker, K., Rondenay, S., Ramalho, R., Thomas, C., & Helffrich, G. (2018). Constraints on the structure of the crust and lithosphere beneath the Azores Islands from teleseismic receiver functions. *Geophysical Journal International*, *213*, 824–835. https://doi.org/10.1093/gji/ggy022

Storch, B., Haase, K. M., Romer, R. H. W., Beier, C., & Koppers, A. A. P. (2020). Rifting of the oceanic Azores Plateau with episodic volcanic activity. *Scientific Reports*, *10*, 1–12. https://doi.org/10.1038/s41598-020-76691-1

Tempera, F., Hipólito, A., Madeira, J., Vieira, S., Campos, A. S., & Mitchell, N. C. (2013). Condor seamount (Azores, NE Atlantic): A morpho-tectonic interpretation. *Deep Sea Research Part II: Topical Studies in Oceanography*, *98*, 7–23. https://doi.org/10.1016/j.dsr2.2013.09.016

Trippanera, D., Porreca, M., Ruch, J., Pimentel, A., Acocella, V., Pacheco, J., & Salvatore, M. (2014). Relationships between tectonics and magmatism in a transtensive/transform setting: An example from Faial Island (Azores, Portugal). *Geological Society of America Bulletin*, *126*, 164–181. https://doi.org/10.1130/b30758.1

Turner, S., Hawkesworth, C., Rogers, N., & King, P. (1997). U-Th isotope disequilibria and ocean island basalt generation in the Azores. *Chemical Geology*, *139*, 145–164. https://doi.org/10.1016/s0009-2541(97)00031-4

Vogt, P. R., & Jung, W. Y. (2004). The Terceira Rift as hyper-slow, hotspot-dominated oblique spreading axis: A comparison with other slow-spreading plate boundaries. *Earth and Planetary Science Letters*, *218*, 77–90. https://doi.org/10.1016/s0012-821x(03)00627-7

Walker, G. P. L. (1999). Volcanic rift zones and their intrusion swarms. *Journal of Volcanology and Geothermal Research*, *94*, 21–34. https://doi.org/10.1016/s0377-0273(99)00096-7

Weiß, B. J., Hübscher, C., & Lüdmann, T. (2015). The tectonic evolution of the southeastern Terceira Rift/São Miguel region (Azores). *Tectonophysics*, *654*, 75–95. https://doi.org/10.1016/j.tecto.2015.04.018

Weiß, B. J., Hübscher, C., Wolf, D., & Lüdmann, T. (2015). Submarine explosive volcanism in the southeastern Terceira Rift/São Miguel region (Azores). *Journal of Volcanology and Geothermal Research*, *303*, 79–91. https://doi.org/10.1016/j.jvolgeores.2015.07.028

Weston, F. (1964). List of recorded volcanic eruptions in the Azores with brief reports. *Boletim do museu e laboratorio mineralogico e geologico da faculdade de ciencias* (pp. 3–18).

White, W. M., Schilling, J. G., & Hart, S. R. (1976). Evidence for Azores mantle plume from strontium isotope geochemistry of central North-Atlantic. *Nature*, *263*, 659–663. https://doi.org/10.1038/263659a0

Widom, E., Carlson, R., Gill, J., & Schmincke, H.-U. (1997). Th–Sr–Nd–Pb isotope and trace element evidence for the origin of the Sao Miguel, Azores, enriched mantle source. *Chemical Geology*, *14*, 49–68. https://doi.org/10.1016/s0009-2541(97)00041-7

Wilson, J. T. (1968). Static or mobile earth: The current scientific revolution. *Proceedings of the American Philosophical Society*, *112*, 309–320.

Yang, T., Shen, Y., van der Lee, S., Solomon, S. C., & Hung, S.-H. (2006). Upper mantle structure beneath the Azores hotspot from finite-frequency seismic tomography. *Earth and Planetary Science Letters*, *250*, 11–26. https://doi.org/10.1016/j.epsl.2006.07.031

Zanon, V. (2015). Conditions for mafic magma storage beneath fissure zones at oceanic islands. The case of São Miguel island (Azores archipelago). *Geological Society, London, Special Publications*, *422*, 85–104. https://doi.org/10.1144/sp422.4

Zanon, V., & Frezzotti, M. L. (2013). Magma storage and ascent conditions beneath Pico and Faial islands (Azores archipelago): A study on fluid inclusions. *Geochemistry, Geophysics, Geosystems*, *14*, 3494–3514. https://doi.org/10.1002/ggge.20221

Zanon, V., & Pimentel, A. (2015). Spatio-temporal constraints on magma storage and ascent conditions in a transtensional tectonic setting: The case of the Terceira Island (Azores). *American Mineralogist*, *100*, 795–805. https://doi.org/10.2138/am-2015-4936